Ultrafiltration membranes modified by PSS deposition and plasma treatment for Cr(VI) removal.

Ivette G. SANDOVAL-OLVERA[1], Pilar GONZÁLEZ-MUÑOZ[1], Laura PALACIO[2], Antonio HERNÁNDEZ[2], Mario ÁVILA-RODRÍGUEZ[1], Pedro PRÁDANOS[2].*

[1]Departamento de Química, Universidad de Guanajuato, Cerro de la Venada s/n, 36040, Guanajuato Gto., Mexico.
[2]Grupo de Superficies y Materiales Porosos, Dpto. Física Aplicada, Facultad de Ciencias, Universidad de Valladolid, 47071, Valladolid, Spain

Declarations of interest: none

Abstract

Ultrafiltration, UF, membranes of positively-charged polyvinylidene fluoride, PVDF, have been modified by the deposition of a layer of poly(styrenesulfonate), PSS, which is negatively charged. These membranes have been treated by radiofrequency plasma at different powers and with different gases (argon, air and carbon dioxide). The membrane treated at 10.2 W with argon gave the best chromate retentions with good stability in water, alkaline and acid media.

Surface zeta potential measurements confirmed the positive surface charge of PVDF membranes, whereas the membranes modified with PSS and argon-plasma treatment had a negative charge in the pH range 3 – 10. FTIR-ATR showed a true grafting of PSS on PVDF for the medium-power argon-treated membrane. SEM pictures of transversal sections confirmed continuity between the PVDF substrate and the PSS layer. The chromium found on the modified membranes confirmed an electrostatically-determined retention. Pore-size distribution, as obtained by image analysis of SEM pictures of the surface, gave a slight reduction of pores but still in the clear ultrafiltration range in accordance with a no-size exclusion mechanism for retention.

The modifications studied led to UF membranes provided with enough negative charges to boost retention of anionic species quite similar to those of nanofiltration membranes but with much lower applied pressures.

Keywords:

Cr(VI) removal; membrane modification; PVDF membranes; argon plasma; ultrafiltration.

* Corresponding author. E-mail address: pradanos@termo.uva.es; Tel: +34 983 42 37 39; Fax: +34 983 42 30 13

Introduction

The increase in industrial and technological activity has brought with it high levels of water contamination. This water contamination has become one of the main global health problems, causing various infections and mortality in all living organisms.

One water contaminant that has attracted a great deal of attention due to its high toxicity in living beings is Cr(VI). In humans it can cause skin irritation and even cancer [1–3]. The main sources of Cr(VI) contamination are derived from anthropogenic activities such as mining, electroplating, pigment production and leather tanning [4,5]. The wastes from these industries are discharged directly into wastewater or, illegally, into rivers, lakes and seas in less-developed countries. Due to the high mobility of Cr (VI) in neutral and alkaline soils, it is often easily incorporated into aquifers [6,7].

The removal and elimination of water contaminants and specifically Cr(VI) is a global priority challenge for the protection of the environment and living beings. That is why the scientific community is making great efforts to find new water treatment methods and technologies for the removal and elimination of Cr (VI). Among the various technologies that have been used in treating water with Cr(VI) we can include precipitation [8], adsorption [9], biodegradation [10], photodegradation [11], reduction [12] and ionic exchange [13].

Gong et al. [14] used iron sulfide-iron coated magnetic nanoparticles (Fe/FeS) for Cr(VI) removal in simulated groundwater. Nanoparticles reduced Cr(VI) to Cr(III). The authors reported that the process had the highest efficiency at pH 3.5 and Cr(VI) solutions at concentrations of 10 mg/L; however, by increasing pH or the Cr(VI) concentration of the solution, its removal decreases by up to 60%.

In the study reported by Yu et al. [15], the removal of Cr(VI) was done by adsorption in microspheres of cellulose functionalized with amino groups. The functionalization was carried out with Gamma radiation. According to their results, the microspheres reached a removal of 129 mg Cr(VI)/g microspheres at pH 3.08. These microspheres had a removal of 91% Cr(VI) in solutions and showed good stability.

Sinha et al. [16] removed Cr(VI) through phytoremediation with the plant *Tradescantia pallida*. The removal was carried out continuously by accumulation of chromium in the roots of the plant. Scale laboratory contaminated water was used in concentrations of 20 and 30 mg/L. The pH effect for each dissolution was studied. The best result for maximum total chromium removal efficiency was 86 – 88.2% achieved at pH 7.

Chen et al. [17] designed a Cr-methanol fuel cell that produces electrical energy from Cr(VI) removal. According to their study, from an initial concentration of Cr(VI) of 3500 mg/L, the concentration decreased more than 91% in a cycle of 400 minutes. The cell can produce up to 903 W/m^2 and can work in a temperature range of -14° C to 45° C.

However, the currently available technologies are usually expensive, produce new toxic by-products and even prove to be inefficient at low concentrations of Cr(VI).

Another option for treating water contaminated with Cr(VI) is separation with membrane technology. Membranes have been widely used in water treatment as they have the ability to concentrate contaminants in a small volume, can be re-used and do not generate toxic by-products.

Membrane technology has also been used in hybrid processes, combining the advantages of membranes with compounds such as clays [18], nanoparticles [19] or microorganisms [20]. In this way, the adsorption and/or reduction advantages of membranes are exploited to design ad hoc technologies for the removal of Cr(VI).

The membrane processes typically used in removal of Cr(VI) are Nanofiltration (NF) and Reverse Osmosis (RO). Since they require small pores (below 1 nm), they are usually quite effective in the removal not only of Cr(VI) but of any ionic species. Their main drawback is that they are the processes that require the highest pressures of membrane processes used in water treatment.

Kazemi et al. [21] modified polyamide nanofiltration membranes with chitosan and iron and titanium dioxide (nZVI@TiO_2) photocatalytic nanoparticles. The modifications were made with the technique known as layer by layer (LBL) and were tested in the removal of Cr(VI). They found that, in the first stage, Cr(VI) was adsorbed on chitosan while, in the second stage, UV light-activated nanoparticles accomplished photodegradation. They obtained chromium removal percentages higher than 95% at pH 2 in Cr(VI) solutions of 10 mg/L.

Gaikwad and Balomajumder [22] studied the simultaneous rejection of fluoride and Cr(VI) with reverse osmosis membranes. Solutions of 5 mg/L and pH 8 were used, while the pressure was 16 bar. They reported that membranes reached rejections of 94.99% for fluoride and 99.97% for Cr(VI) under those conditions.

On the other hand, Ultrafiltration (UF) is among the membrane processes that require the lowest pressures. The main application of UF is to separate high-molecular-weight contaminants such as peptides and polysaccharides. Due to their pore size, UF membranes are not able to carry out the separation of ionic species. However, they can be modified by acquiring characteristics of NF membranes, for example, the ability to separate small ionic species. At the same time, they retain the need of only relatively low pressures during separation, which is a characteristic of UF. Therefore, modified UF membranes are a new alternative in the treatment of water contaminated with Cr(VI) or ionic species.

Yao et al. [23] modified polyvinylidene fluoride (PVDF) ultrafiltration membranes with polymers with tertiary amino and quaternary ammonium groups for Cr(VI) removal. The membranes acquired a positive charge after modification, so the key separation mechanism was adsorption. The membranes had a Cr(VI) uptake of 63.17 mg/g at pH 7. The concentration of the solutions was 10 mg $K_2Cr_2O_7$/L and the pressure, 1 bar. The authors concluded that these membranes can be applied for low concentrations of Cr(VI).

Gebru and Das [24] made cellulose acetate UF membranes modified by impregnation of different polymers with amino groups and nanoparticles of titanium dioxide within the membrane structure. The membranes were used in Cr(VI) removal and, according to their results, the separation mechanism was through electrostatic interactions of attraction between the positive amino groups and the negative Cr(VI) at pH 3.5, whereas, at pH 7 the separation was by electrostatic repulsions

between the negatively-charged titanium dioxide nanoparticles and negative Cr(VI). The membranes showed the best performances at pH 3.5 and a Cr(VI) concentration of 10 mg/L.

As can be seen, there are many membrane modification techniques. With surface coating, a new layer is deposited on the active layer of the original membrane [25]. This new layer usually consists of nanoparticles or some monomer or polymer that causes a change in the surface charge density or the wettability of the membrane surface. This produces a reduction of fouling and/or an increase in retention. The main drawback of surface coating techniques is that, if there is not a grafting process, the duration of the modification is far too short [26] for most relevant applications.

For its part, plasma treatment can consolidate previously adsorbed or deposited layers "in situ." This technique works with gaseous or vapor phase reactives; it is easy to use and especially suitable for creating new layers on a membrane. Therefore, plasma treatment can cause uniform and permanent grafting of the modifying agent [27,28]. When a polymer is used, the built layer keeps its chain mobility and functional groups [29]. In our case, we will focus on plasma generated by inorganic gases. It is known that this way of using plasma can induce crosslinking or chain disruption and, in some cases, even the appearance of new functional groups [30].

This paper proposes Cr(VI) removal from synthetic solutions through modified ultrafiltration membranes. Positively-charged PVDF membranes will be coated with negatively-charged sodium polystyrenesulfonate (PSS); subsequently, they will be treated separately with the plasma of several inorganic gases. After the modification, the negatively-charged membranes will be shown to have achieved good removal of Cr(VI), and to have good stability after 5 weeks. In addition, they will be tested for the removal of other anions. They will be shown to retain nitrates and acid chromates with acceptable results, as well as to have a good separation rate of phosphate mixtures. Therefore, these membranes will be proved to have good potential for the removal of contaminant anions.

1. Experiment

1.1. Materials and Chemicals

Ultrafiltration PVDF (polyvinylidene difluoride) membranes (HFM-183, Koch Membrane Systems, Wilmington, MA, USA) were used. These membranes are claimed by the manufacturer to be positively charged and to have a 100 KDa MWCO (molecular weight cut off). Hereafter, they will be called HFM-183 membranes.

Their water permeability, as measured by us, was $(8.09 \pm 1.57) \cdot 10^{-10}$ m/Pa·s, as obtained from 15 experiments. PSS (poly(styrenesulfonate)) of a molecular weight Mw=70,000 Da, which was tested to modify the PVDF membranes, was bought in a 30 % w/w water solution from Sigma Aldrich (Sigma-Aldrich, St. Louis, Missouri, USA).

The other chemicals (potassium dichromate, sodium nitrate, monosodium phosphate (anhydrous), potassium chloride, hydrochloric acid, sodium hydroxide, glycerol, sulfuric acid, antimony potassium tartrate, ammonium molybdate and ascorbic acid) were acquired at analytical grade from Sigma-Aldrich as well. Ultrapure (ASTM Type I) water was always used.

All filtration tests and experiments were performed on a flat membrane dead-end device (HP4750, Sterlitech Co., WA, USA). Each membrane sample was used as a 14.6 cm^2disc. Nitrogen was used to pressurize.

1.2. Membrane Modifications

50-mm diameter discs of the HFM-183 membrane were first cleaned with water. Thereafter, 50 mL of differently concentrated aqueous PSS (Mw=70,000 Da was selected because it gave better results) solutions were filtered through the HFM-183 membrane under a pressure drop of 8 bar. Several concentrations of PSS were initially tested. No stirring or natural pH was used in order to allow a uniform deposition. Right away, the membranes were soaked in glycerol and placed in an oven at 35 ˚C for 1 hour.

After testing chromate retention and volume flux under conditions detailed in the next section, a 20.8 g/L PSS water solution was chosen and subsequent experiments were performed for this concentration only. Concentrations over 20.8 g/L did not result in significantly higher retentions while substantially smaller water permeability was obtained. Consideration of the mass balance in the experimental PSS deposition by permeation of the 20.8 g/L aqueous solution suggested that there were 71 mg of PSS/cm^2 on the membrane.

Afterwards, plasma treatments were performed in a radiofrequency plasma chamber (Expanded Plasma Cleaner PDC-001, Harrick Plasma, Ithaca, NY, USA) connected to a flux mixer (PlasmaFlo PDC-FMG, Harrick Plasma, Ithaca, NY, USA) and a vacuum pump. Three gases were used: air, argon and carbon dioxide in a flux of 0.30 cm^3/min STP. Three powers were set: 7.2, 10.2 and 29.6 W for 15 min. These powers, gases and treatment times were selected according to previous experiments [31]. All experiments were performed in triplicate.

1.3. Functional Characterization

1.3.1. Anionic Separation

After modification, the water permeability, L_p, was measured. The volume flux, J_V, and the observed retention, R_{obs}, of four cationic solutions— chromates, acid chromates, nitrates and a mixture of acid and diacid phosphates— was also measured. In this case, pH was controlled to assure the dominancy of each ionic species. A pH 8 was used for all the species except for the acid chromates that required a pH 4. To measure volume flux and retention, a 30 mg/L concentration was used, and an initial 100 mL of the corresponding solution was filtered, at a stirring speed of 180 rpm and a pressure of 3 bar, and successive samples of 10 mL permeate were gathered and their concentration measured. In order to guarantee a stationary state, the first 10 mL of permeate were cast aside.

Observed saline retention could be evaluated as:

$$R_{obs} = 1 - \frac{\overline{C}_p}{\overline{C}_f} \quad (1)$$

$\overline{C}_f$ and $\overline{C}_p$ are the average feed and permeate concentrations for the last five 10-mL permeate samples. $\overline{C}_f$ was obtained by a detailed mass balance for all the permeated samples. In the same way, J_V corresponded to averages for the last 5 permeate samples. All measurements were performed threefold.

1.3.2. Ionic Concentrations

All concentrations were quantified by using UV-Vis spectrometry (UV-160A, Shimadzu, Kyoto, Japan). For chromium, a wavelength of 373 nm was used [32]. For nitrates, the wavelength was 220 nm [33]. Concentrations of phosphate species were evaluated at 800 nm [34].

1.3.3. Modification Stability

Once the modified membranes were functionally tested, they were immersed in water for two weeks. After this period of immersion, water permeability, observed retention of the ionic solution and volume flux were evaluated again. After two more weeks immersed in water they were immersed in a $1 \cdot 10^{-4}$ M NaOH solution for 24 hours and functionally tested again. Finally, the membranes were kept in a 1×10^{-3} M HCl solution for 24 hours and L_p, J_V and R_{obs} measured for a third time.

1.4. Morphology, Electrical and Chemical Characterization

1.4.1. Zeta potential

The Zeta Potential, ζ (SurPASS, Anton Paar, Austria) was measured on the surface of the HFM-183 membrane, the modified HFM-183-PSS membranes and HFM-183-PSS + Ar-medium.

In each analysis, a pair of 10 x 20 mm membrane pieces were used. The measurements were carried out in a 1×10^{-3} M potassium chloride medium, with an initial volume of 500 mL. A pH measurement interval of 3 – 10 was used. For each sample, the titration was performed at basic and acid pH with sodium hydroxide and hydrochloric acid respectively. The initial pH of each titration was the solution of potassium chloride (pH 5.7). The experiments were carried out in triplicate.

1.4.2. Scanning Electron Microscopy (SEM)

Scanning Electron Microscopy (SEM) (SIGMA-HDVP Field Emission, Carl Zeiss, Oberkochen, Germany) was used to observe the surface and transversal sections of both the modified and unmodified membranes.

For the surface studies, discs of 20 mm of diameter were lyophilized to protect their porous structure; subsequently, 0.5-cm^2 samples were cut and gold-coated for 1 min. Transversal sections

were performed by immersing the lyophilized samples in liquid nitrogen for 5 min and cutting with a scalpel. The samples were finally gold-coated once again for 1 min.

Pore-size distributions were observed from SEM pictures at 20,000 magnification and with the computerized image analysis performed by using the ImageJ software. From surface features, the equivalent circular pore diameters (Feret diameters) were evaluated and their statistics evaluated.

1.4.3. *Energy-dispersive X-ray Spectroscopy (EDS)*

The elemental analysis of unmodified and modified membranes was performed by an X-ray sensor equipped with high efficiency XFlash 6 detectors (QUANTAX, Bruker, Billerica, MA, USA) coupled to the SEM device used.

1.4.4. *Attenuated Total R*eflectance *Fourier Transform Infrared Spectroscopy (FTIR-ATR)*

FTIR-ATR was performed by using a PerkinElmer RX-1 spectrometer with a Universal ATR Sampling Accessory Module (Perkin Elmer, Boston, MA, USA). It was used to identify the main functional groups on the surfaces of all the membranes. Measurements were done with a spectral resolution of 4 cm^{-1} and 16 scans. Diamond ATR crystals were used.

For the sake of comparison, a pure PSS film was measured as well. It was manufactured from the 30% water solution by allowing a 5 mL layer to evaporate on a hot plate.

2. Results and Discussion

2.1. Functional Membrane Characteristics

2.1.1. *Membrane Modifications*

Different conditions of plasma treatment were tested. The membranes and conditions of plasma treatment are detailed in Table I.

Table I. Plasma treatment conditions and membranes.

Gas	Power (Watt)	Time (min)	Label
---	---	---	HFM-183+PSS
Argon	7.2 (low)	15	HFM-183+PSS + Ar-low
Argon	10.2 (medium)	15	HFM-183+PSS + Ar-medium
Argon	29.6 (high)	15	HFM-183+PSS + Ar-high
Air	10.2	15	HFM-183+PSS + Air-medium
Carbon dioxide	10.2	15	HFM-183+PSS + CO_2 -medium

2.1.2. *Membrane Performance in Chromate Retention*

In order to analyze the functional characteristics of the modified membranes, we started with permeate chromates at pH 8 (where, in effect, the chromate ion is dominating the electrochemical

equilibrium). In Table II, the water permeability, L_p along with the filtration volume flux, J_V, and observed retention, R_{obs}, are shown.

Table II. Water permeability and chromate volume flux and observed retention.			
Membrane	L_p (10^{-10} m/Pa s)	J_V CrO_4^{2-} (10^{-5} m/s)	R_{obs} (%)
HFM-183+PSS	1.31 ± 0.10	4.30 ± 0.18	58.35 ± 3.50
HFM-183+PSS + Ar-low	0.94 ± 0.05	3.15 ± 0.06	60.38 ± 0.92
HFM-183+PSS + Ar-medium	0.65 ± 0.01	2.28 ± 0.31	66.01 ± 1.42
HFM-183+PSS + Ar-high	1.01 ± 0.15	3.61 ± 0.04	57.40 ± 2.86
HFM-183+PSS + Air-medium	1.30 ± 0.18	4.57 ± 0.36	44.93 ± 1.44
HFM-183+PSS + CO_2 -medium	1.16 ± 0.04	5.02 ± 0.10	44.38 ± 1.42

It can be seen that the membranes coated only with PSS have the best water permeability with a high volume flux and a retention that is not too low. It is worth mentioning that retention for the pristine HFM-183 was close to zero.

The membranes treated in air and carbon dioxide showed high water permeability and volume flux, actually both quite similar to the HFM-183+PSS without any plasma treatment but with lower retentions. It seems clear that these plasma treatments are inefficient or even detrimental. These gases would graft beneficial groups (hydroxyl for air and carboxyl for CO_2, [35]) and cause crosslinking, but they can also roughen the membrane surfaces (with degradation or even etching) and neutralize existing charged groups. Both of these effects would decrease retention while increasing permeability, as effectively seen in our case.

It appears clear that argon-plasma treatments increase retentions at the expense of decreasing permeability and chromate flux. Argon is known to generate free radicals on the surface of a polymeric substrate with likely subsequent crosslinking. Among the argon plasma-treated membranes, the medium power seems to be advisable inasmuch as it gives the highest retention. The existence of maximal retention at intermediate powers would mean that there is a roughening effect that would oppose, and eventually cancel out (or even dominate as it is probably the case for HFM-183+PSS+ Ar-high), the advantageous creation of free radicals and crosslinking.

Data in Table II show that there is an approximate inverse correlation between observed chromate retention and its volume flux. This trend is shown in Figure 1, where a straight line has been fitted and the 95 % confidence interval shown.

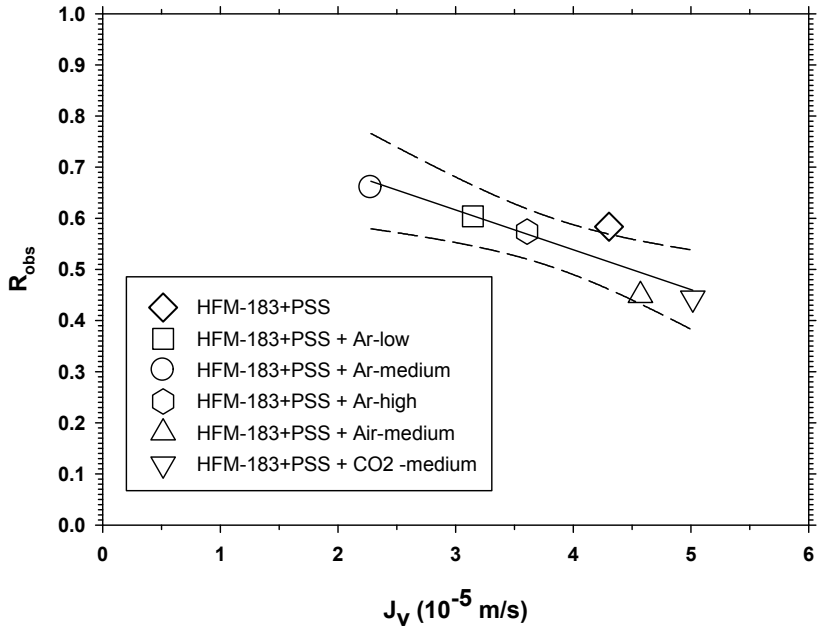

Fig. 1.- Observed retention versus volume flux of chromate solutions for different plasma treatments. Lines correspond to the best straight line fitting the data.

2.1.3.*Stability of Modified Membranes*

In order to evaluate the stability of the treatments, they were immersed in water for two weeks. After two more weeks of water immersion, they were submerged for 24 hours in a basic solution and immediately afterwards in an acidic bath for 24 additional hours.

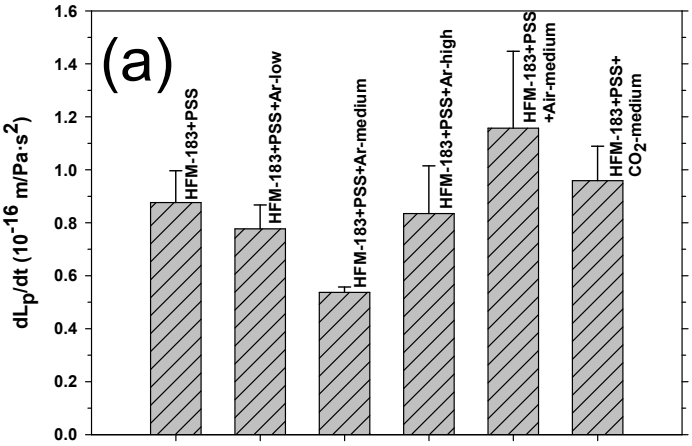

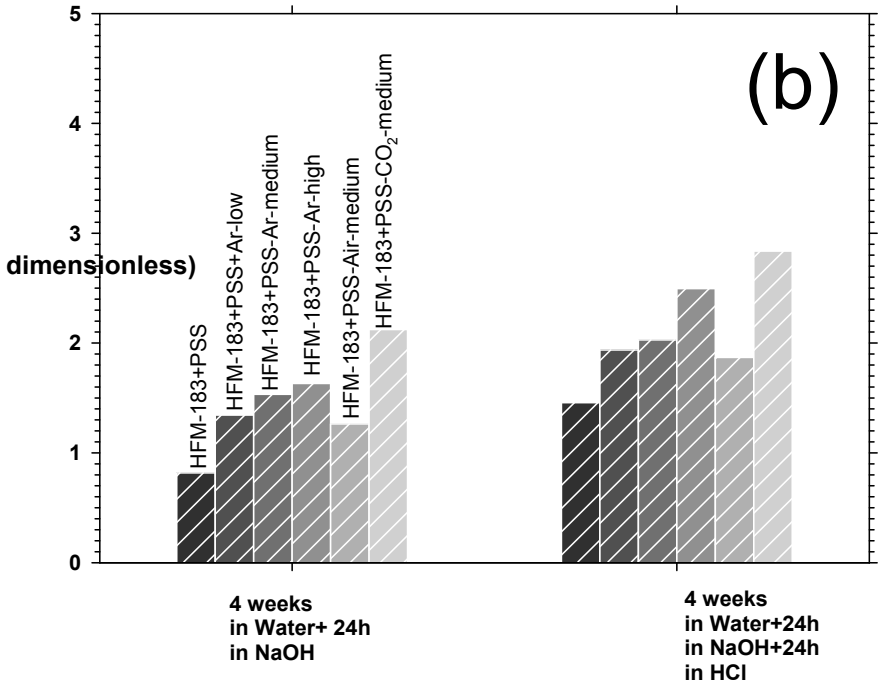

Fig. 2.- a) Water permeability rate of change due to water immersion b) Relative changes in water permeability after alkaline and acidic treatments for different plasma treatments.

The changes in permeability with the time of water immersion are shown in Figure 2-a. It seems clear that the membranes treated with Ar plasma at an intermediate power show the highest stability. This means that at this power, crosslinking most likely predominates over the inconvenient thinning (with loss of material) characterizing the phenomenon at higher powers. In Figure 2-b, the corresponding relative changes of water permeability due to alkaline and acid immersions are shown.

In all cases, there is an increase of water permeability, probably due to a slight loss of initially-deposited polymer chains. When hydroxyl groups or protons are present, the structure of the membranes is loosened again, leading to increasing permeability. Especially fragile structures (high water permeability increases) appear for CO_2 or high-power plasma treatments. Similar permeability intensifications appear for low or medium-power argon-plasma treatments. It is notable that, even though the HFM-183+PSS membrane without any plasma treatment suffers the least change in permeability, its stability in water is lower than that of any other plasma-treated membrane.

As seen in Table II, there is a clear direct proportionality between water permeability and chromate volume fluxes. This trend is preserved after stability tests as shown in Figure 3. It is worth mentioning here that the reproducibility, considering the corresponding error bars, of the

membranes treated with argon-plasma at these low and medium powers is higher than that of all the other cases.

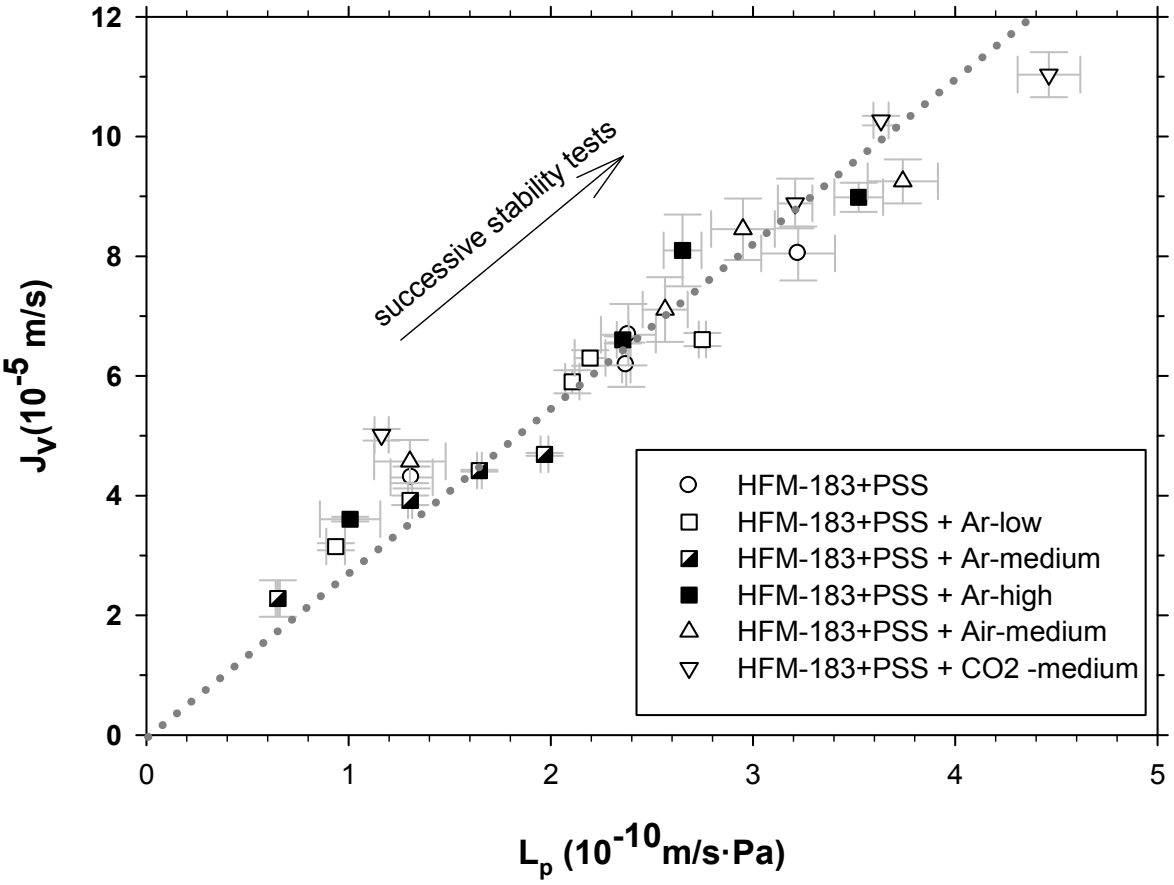

Fig. 3.- Chromate volume fluxes versus water permeability.

The inverse relationship between observed retention and volume flux is quite logical. Similar trends have been identified between permeability and selectivity in gas separation using membranes, where Robeson plots have acquired an almost standard character [36]. This kind of double-log representation can also be of great help here. In Figure 4, such a log-log plot of observed retention as a function of chromate flux is shown for the untreated membranes before and after their treatments to test stability. The line drawn in this figure would correspond to the apparent best performance between retention and permeate flux.

It seems clear that before the described tests for stability, only the argon plasma-treated membranes and the untreated ones showed more than 0.5 observed retention. The HFM-183+PSS membrane quickly goes down to this retention level after being immersed in water, and immersion in NaOH or

HCl does not make things better. Among the argon plasma-treated membranes, only that of a medium-power plasma remained over this arbitrary 50% retention limit.

For their part, the air or CO_2 plasma-treated membranes show lower initial retentions that decrease deeply after their immersion in water. It seems that air-plasma treatments can lead to new functional groups that after alkaline hydrolysis generate more negative charges [35]. This could be also the case after acidic treatment. In these cases, it is worth noting that the alkaline and acid treatments recover some retention with simultaneous increases in permeability. Although this increase in permeability might be correlated to a certain elimination of material (etching), it is also probable that alkaline immersion of CO_2-treated membranes would create -COOH groups, while in the case of air plasma-treated membranes, –OH groups could appear. Both of these groups would increase retention of anions. For the argon-treated membranes, alkali and acid would only have some etching actions that would mainly increase permeability.

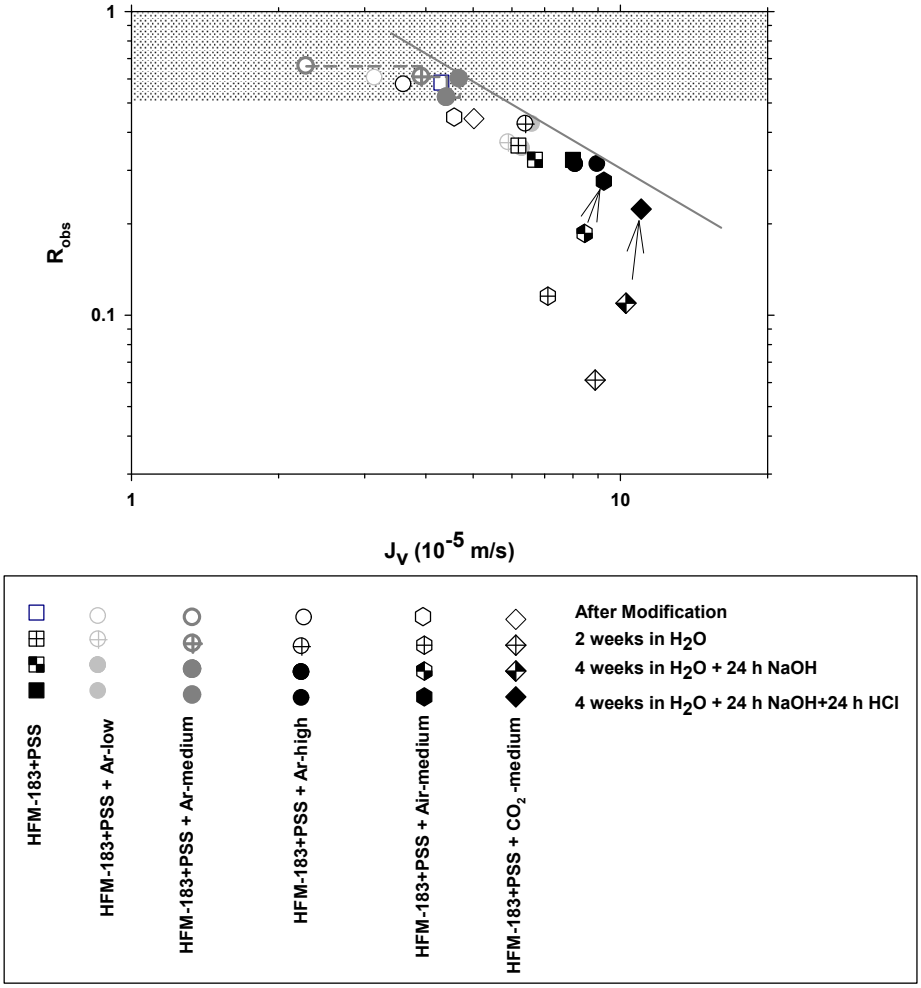

Fig. 4.- Observed retention versus volume flux of chromate solutions for the different plasma treatments before and after their tests for stability.

In any case, it seems clear that argon-plasma treatment at intermediate powers stabilizes the membrane allowing it to keep the best compromise of retention and permeability after the successive treatments. The Ar plasma is probably able to produce radicals that can increase crosslinking of both the PSS layer and the PVDF substrate of the pristine HFM-183 membrane while higher powers would cause some elimination of material from the surfaces with some possible etching as well.

2.1.4. Membrane Performance for other Anions

HFM-183+PSS+Ar-medium membranes were used to filtrate different anionic solutions, namely nitrate solutions at pH 8, acid chromate at pH 4 and a mixture of phosphates $H_2PO_4^-$/ HPO_4^{2-} at pH 8. Some properties of these anions are shown in Table III. r_{anion} is the molecular radius (thermochemical radius) of the anion.

Table III. Data, [37–40], for the ions permeated.

Species	r_{anion} (pm)	MW (g/mol)	Elemental charge	Geometry	D (10^{-9} m^2/s)
NO_3^-	179	62.00	-1	Flat triangular	1.53
$HCrO_4^-$	240	117.00	-1	Tetrahedral	1.20
CrO_4^{2-}	256	116.00	-2	Tetrahedral	1.39
$H_2PO_4^-$	200	96.99	-1	Tetrahedral	0.80
HPO_4^{2-}	238	95.98	-2	Tetrahedral	0.86

In Figure 5, the observed retentions for these anionic solutions are shown versus the volume flux in a double-log plot. They are shown for the HFM-183+PSS+Ar-medium membrane and compared with that of chromate. The straight line drawn here is the same as the one in Figure 4. Although these retentions are not high, and all of them are below that of chromate, which is around 66 %, it is worth noting that they are observed retentions that are known to be lower than the membranes' true retentions that take into account the concentrations directly in contact with the membrane, isolating the effects of polarization that could be decreased, and the true retention approximated, by increasing stirring or decreasing working pressures and concentrations.

The mass transfer coefficient of the cell can be evaluated by [41]:

$$k_m = A r_c^{2\alpha-1} \rho^{\alpha-\beta} \eta^{\beta-\alpha} D^{1-\beta} \omega^{\alpha} \quad (2)$$

where A =0.241 for the cell used, r_c =25.5 mm is the radius of the circular cell, $\alpha = 0.75$ and β =1/3 are the Sherwood correlation parameters, ρ and η are density and viscosity (assumed to be

those of water), D is the ionic diffusivity and ω is the angular speed of stirring. Thereafter we can get true retention R from observed retention R_{obs} by:

$$\ln\left(\frac{1-R}{R}\right) = \ln\left(\frac{1-R_{obs}}{R_{obs}}\right) - \frac{J_V}{k_m} \tag{3}$$

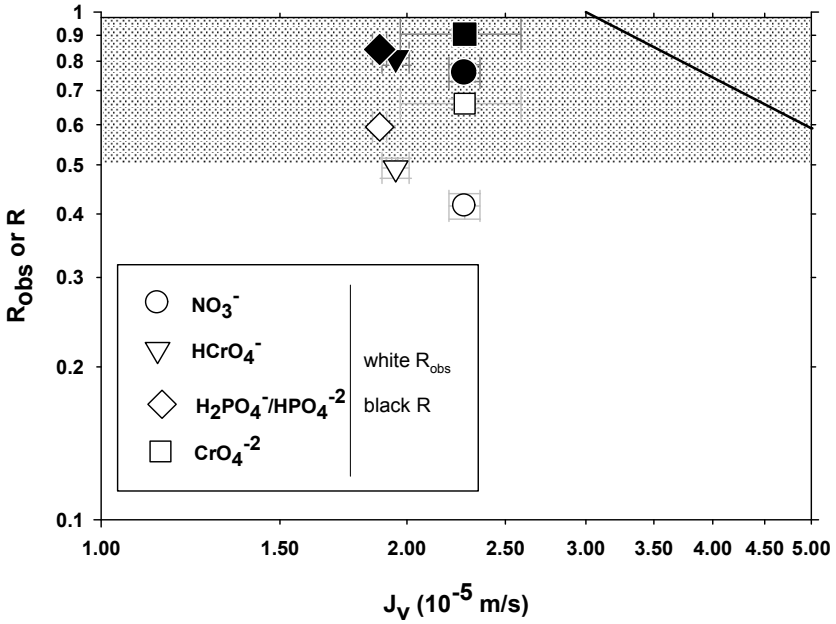

Fig. 5.- Observed and true retention for the HFM-183+PSS+Ar-medium membrane and the anionic solutions used.

These true retention coefficients are shown in Figure 5, along with R_{obs}. It can be seen that true retentions, in effect, increase substantially when compared with the observed ones, reaching 91% for chromate, which strongly suggests that a better filtration system design would raise membrane productivity. For the solutions studied, all volume fluxes are quite similar although retentions cover a much more significant range. Nitrate is the least retained anion tested. This is not surprising as it is the smallest one; it has a flat triangular structure. Nitrate has also the highest diffusivity and, accordingly, the highest mass transfer coefficient. The acid chromate anion, although it has the same charge, is retained more because it is bigger and tetrahedral. Chromate, although sharing geometry with the acid chromate anion, is slightly bigger and doubles the charge of the acid chromate ion; thus it is retained quite well by the HFM-183+PSS+Ar-medium membrane. It is worth noting that these filtration experiments with acid chromates were conducted at pH 4 and show similar retentions (similar charges) to those for CrO_4^{2-} done at pH 8. This means that the

modified HFM-183+PSS+Ar-medium membrane is most likely negative at pH ranges from 4 to 8 at least.

Finally, the $H_2PO_4^-/HPO_4^{2-}$ mixture in size and structure is similar to $HCrO_4^-$ but it is retained quite well due to its charge.

2.2. Membrane Material Characteristics

2.2.1. Zeta Potential

The surface zeta potential, ζ , was measured on the pristine HFM-183 membranes, as well as on the modified ones, HFM-183+PSS and HFM-183+PSS+Ar-medium. The results of these measurements are shown in Figure 6.

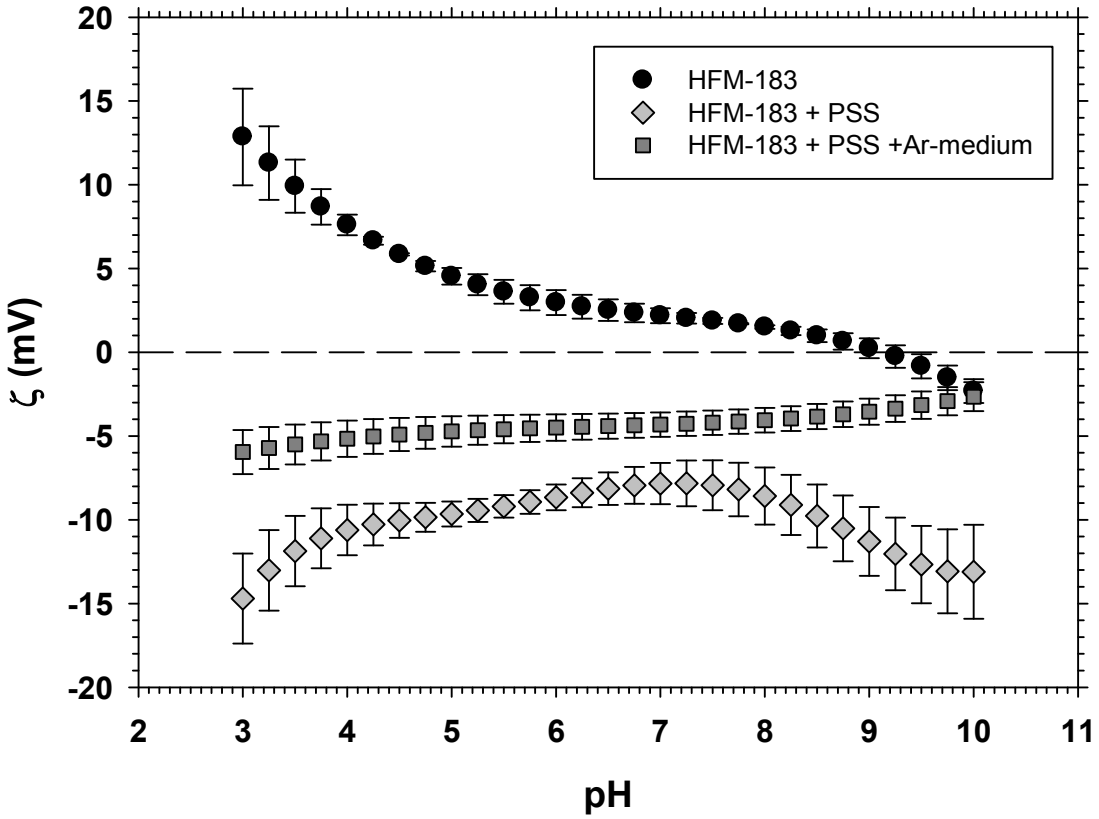

Fig. 6.- Zeta potential vs. pH.

According to Figure 6, the HFM-183 membranes have a positive charge in almost the entire pH window analyzed; there is an isoelectric point at pH 9.12 and a negative charge up to pH 10. The manufacturer reports that they are positive without mentioning the pH or temperature conditions. In any case, the membrane appears to be positive in a wide pH range.

The modified HFM-183 + PSS membranes had a negative charge throughout the pH range analyzed. The reversal of positive-to-negative charge was due to the deposition of PSS. According to our hypothesis, the membrane has a positive charge, while the PSS has a negative charge, thus favoring PSS deposition.

On the other hand, these membranes had the highest standard deviations, as seen in Figure 6, which increased to extreme pH, 3 and 10. This increase of dispersions corresponds experimentally to the end of each titration, basic and acidic. Tangential pressure was applied during the measurement, so it is likely that the increase in dispersions is associated with a gradual removal of the PSS deposited on the membrane. In addition, the pH change during the measurement along with the addition of new ions to the system could have caused the destabilization of the PSS initially deposited, favoring its removal from the surface of the membrane.

The results of zeta potential measurements of HFM-183+PSS membranes are in accordance with those observed in the characterizations of functional performance and stability (Sections 3.1.2 and 3.1.3). The negative charge of the HFM-183+PSS membranes favored the initial retention of chromates, while the low stability of the deposited PSS justifies the progressive fall in the chromate retentions, as well as the increase in water permeability and chromate flow during stability tests.

HFM-183+PSS+Ar-medium membranes are negative through all the measured pH range. These membranes had a lower negative load and lower standard deviations than the HFM-183+PSS membranes.

The decrease of the negative charge and the increase of the stability can be due to the treatment with medium-power argon plasma that these membranes received. Plasma treatment favors crosslinking of the PSS polymer chains, as well as their grafting on the surface of the PVDF membrane [42–44]. That is why the negative charge is lower than on the HFM-183+PSS membranes. However, it also possible that plasma affects the sulfonate functional groups, which are responsible for the negative charge of PSS, and thus reduces the negative charge. Grafting would favor the stabilization of PSS on the surface of the membrane, which explains the small standard deviations.

These results agree with those observed in Sections 3.1.2, 3.1.3 and 3.1.4. The negative charge of HFM-183+PSS+Ar-medium membranes led to their performance in the separation of tested anions, while the stability of PSS on the pristine membrane caused by argon-plasma treatment kept retention, flux, and permeability practically constant with successive stability treatments.

2.2.2. SEM Pictures

Several transversal sections were analyzed by SEM. Some examples are shown in Figure 7. In Figure 7a, a cut of the membrane HFM-183 is shown, providing evidence of how continuous and uniform it is. In Figure 7b, an HFM-183+PSS section is shown. Here a PSS layer can be seen clearly on the original active layer of the HFM-183. The discontinuity between both of these layers can be attributed to the mainly electrostatic character of the adhesion of positive PVDF and negative PSS. A transverse cut of the HFM-183+PSS+Ar-medium is displayed in Figure 7c, showing a not-so-clear separation between PVDF and PSS, probably due to the grafting of PSS on PVDF caused by the argon-plasma treatment.

Figures 7d and 7e, present transversal sections of HFM-183+PSS+Ar-medium membranes after filtration of chromate and acid chromate, respectively. Both of these images share many features with that of Figure 7c. Notable is the case of figure 7d that shows a membrane that after filtration of chromates was immersed in water for 4 weeks and in NaOH for 24 hours, followed by another 24 hours in HCl. These features of Figures 7d and 7e show that their modifications were morphologically quite stable.

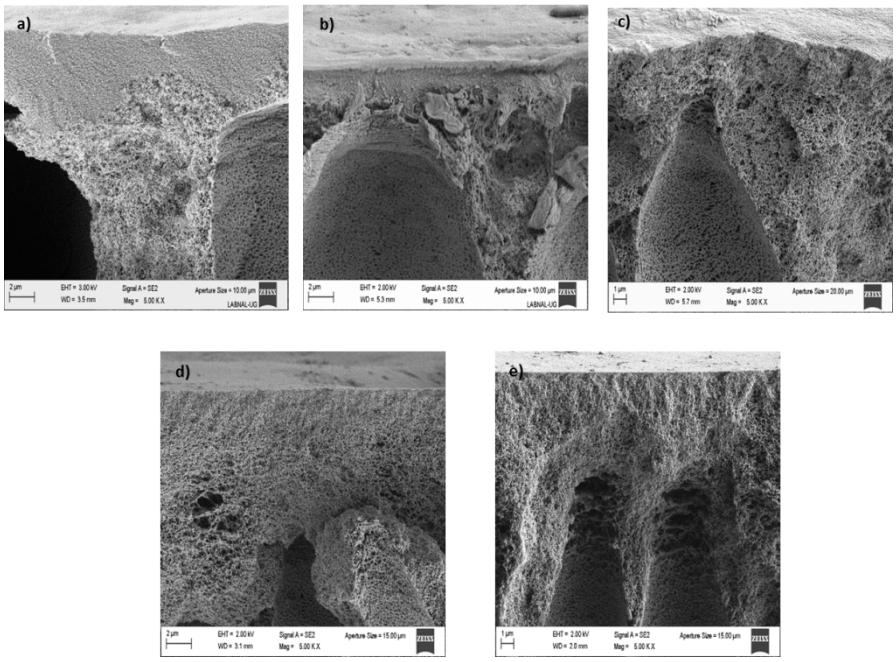

Fig. 7.- SEM pictures of transversal sections of: a) HFM-183, b) HFM-183+PSS, c) HFM-183+PSS+Ar-medium, d) HFM-183+PSS+Ar-medium after chromate filtration and e) HFM-183+PSS+Ar-medium after $HCrO_4^-$ filtration.

2.2.3. *Pore Size from Computerized Image Analysis*

From SEM images of the surfaces of the membranes like those shown in Figure 8, the pore-size distributions (actually, the pore-size distribution of pore openings) can be obtained by computerized image analysis.

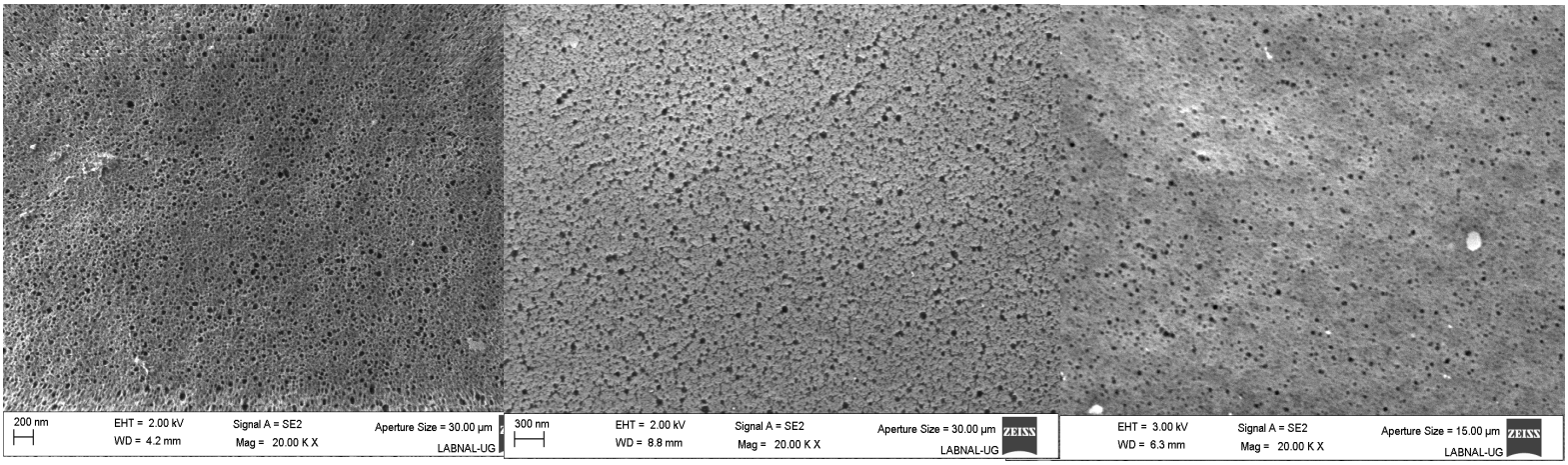

Fig. 8.- Surface SEM image for the membranes: HFM-183 (left), HFM-183+PSS (center) and HFM-183+PSS+Ar-medium (right).

It can be seen from these images that the HFM-183 membrane shows sharper definition of the pore borders. Moreover, the HFM-183+PSS membrane clearly has a less compact appearance than the HFM-183+PSS+Ar-medium.

After image analysis, pore-size distributions appeared quite asymmetric with long wide-pore tails. Thus, they have been fitted to log-normal distributions as shown in Figure 9. It is worth noting that although the wide-pore tails remain unchanged for all the three membranes studied (HFM-183 (left), HFM-183+PSS (center) and HFM-183+PSS+Ar-medium), there is a slipping of the distributions' maxima to markedly narrower pores. In any case, the MWCO of the pristine HFM-183 membrane would correspond to a pore radius of around 15 nm [45]. Given that the membranes, as a result of our modifications, show quite similar wide-pore tails, we can conclude that the size effects would be insufficient by themselves to explain the retentions obtained.

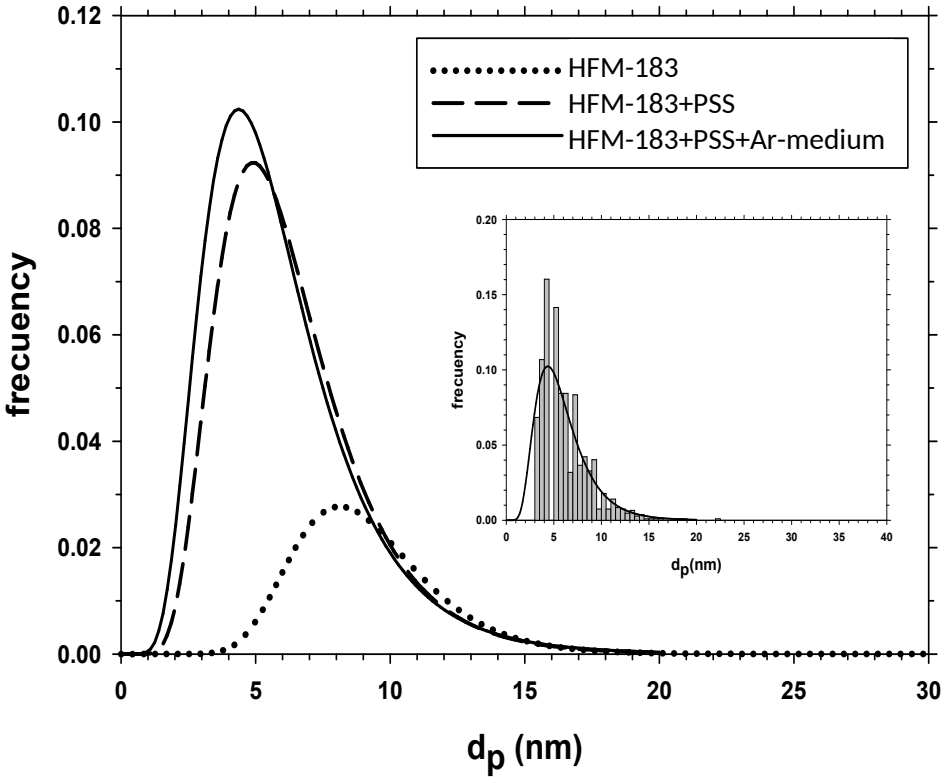

Fig. 9.- Log-normal fitted distribution. The insert shows raw and fitted data for the HFM-183+PSS+Ar-medium membrane.

In Table IV, the statistical parameters for the pore-size distributions presented in Figure 9 are shown. The decrease of mean pore sizes might be a consequence of tight linkage of PSS on PVDF and of the crosslinking induced by intermediate-power argon-plasma modifications. Nevertheless, the size of the anions (according to Table III they have diameters below 0.5 nm) does not justify their retentions, which, in consequence, must be determined by electrostatic interactions. So along with the results of zeta potential we can conclude that the separation mechanism is influenced more by electrostatic interactions than by the pores' size. The electrostatic relevance in retention is distinctive for nanofiltration.

Table IV. Statistical parameters for the log-normal pore size distributions shown in Figure 9.	
Membrane	$\mu \pm \sigma$ (nm)
HFM-183	8.90 ± 0.30
HFM-183+PSS	5.80 ± 0.40
HFM-183+PSS+Ar-medium	5.40 ± 0.50

2.2.4.*Energy-dispersive X-ray Spectroscopy (EDS)*

In order to study the elemental composition of the membranes it is worth considering that the electron beam can penetrate below the surface of the sample. A simulation performed and analyzed using the apparatus software suggests that electron beams in the 20 to 30 kV range can penetrate as

far as 500 nm below the membrane samples. The percentages of several elements detected by EDS are shown in Table V.

Table V. Elemental analysis by EDS of the samples of Figure 7.

	Percentage				
Element	HFM-183	HFM-183-PSS	HFM-183+PSS+Ar-medium	HFM-183+PSS+Ar-medium after CrO_4^{2-} permeation	HFM-183+PSS+Ar-medium after $HCrO_4^-$ permeation
Carbon	64.4 ± 3.2	51.7 ± 2.6	55.6 ± 2.8	63.2 ± 3.2	64.4 ± 3.2
Fluoride	24.2 ± 1.2	32.2 ± 1.6	26.7 ± 1.3	27.1 ± 1.4	25.3 ± 1.3
Oxygen	7.39 ± 0.37	9.56 ± 0.48	10.4 ± 0.5	4.14 ± 0.21	4.13 ± 0.21
Nitrogen	3.33 ± 0.17	2.59 ± 0.13	2.62 ± 0.13	2.50 ± 0.12	2.50 ± 0.12
Sulfur	0.31 ± 0.02	2.43 ± 0.12	2.49 ± 0.12	2.11 ± 0.11	2.13 ± 0.11
Chloride	0.33 ± 0.02	0.03 ± 0.01	N.D.	N.D.	N.D.
Aluminum	0.04 ± 0.01	0.37 ± 0.02	0.25 ± 0.01	0.04 ± 0.01	0.02 ± 0.01
Sodium	N.D.	1.16 ± 0.06	1.88 ± 0.09	0.83 ± 0.04	0.99 ± 0.05
Potassium	N.D.	N.D.	N.D.	0.12 ± 0.01	0.50 ± 0.01
Chrome	N.D.	N.D.	N.D.	0.01 ± 0.01	0.02 ± 0.01

N.D. = Not detected.

PVDF should give a carbon-to-fluoride relation of C/F=1 (-$[CH_2$-$CF_2]_n$-), i.e. 50% C as observed in membranes made out of pure PVDF [46]. In the case of the pristine membrane HFM-183, some other elements appear, displacing this percentage. These elements are: oxygen, sulfur, chloride, nitrogen and aluminum. The C-F asymmetry (C/F=2.7) can be due to the effect of the support membrane (probably polysulfone or polyethersulfone) and the modification of PVDF to make it positive (possibly quaternary ammonium groups that justify the presence of N). Both of these factors-would explain the increase in C and the presence of O, N and S. Cl can play the counter-ion role for the net positive charge of the membrane. With regard to the small aluminum content, it can be attributed to the fabrication process or alternatively to the sample preparation. Many different procedures have been used to get positively-charged PVDF membranes, [47–51]. It is worth noting that the changes in the C/F composition could be due to some changes of the functional groups on the surface, but they can also be caused by the electron-beam penetration into the support membrane.

The HFM-183+PSS membrane has a more symmetric C/F relation of 1.6. It is worth noting that assuming that PVDF would contribute 32.2 % of C (C/F =1), and once this amount of carbon was subtracted and after renormalization, the composition, which should be attributed exclusively to PSS, would be C=62%, O=30% and S=7.7%. This compares well with the theoretical composition of PSS (C=66.66%, O=25% and S=8.33%). This would be the case if we were detecting a 32.2 %

contribution of the PVDF of the pristine HFM-183 that would act now as a substrate of the PSS layer of the HFM-183+PSS. In this case the electron beam could not penetrate into the original support of HFM-183. The small increase of O content over the theoretical one could be due to the positive charging of the HFM-183 membrane. The reduction of the nitrogen content is compatible with the addition of the PSS. Chloride content falls, which can be due to the absence of positive charges to be balanced. Because now that there are negative charges on the PSS, the counter-ion role is played by Na, which is, in fact, present in a small proportion.

The HFM-183+PSS+Ar-medium membrane has a composition quite similar to that of the HFM-183+PSS membrane. Now there is 27.45 % of F; if the same amount of C was subtracted and after renormalization, the composition, which should be attributed exclusively to the PSS, would be C=69%, O=25% and S=6%. This composition would be not far from the theoretical one for PSS. This would mean that now the electron beam would penetrate less through the more compacted (crosslinked) PSS layer. Chloride is now undetectable and sodium increases as far as it would be empowered as a counter-ion of the only negative charges remaining.

Both of the HFM-183+PSS+Ar-medium membranes after CrO_4^{2-} and $HCrO_4^-$ permeation show quite similar compositions. Oxygen and sulfur compositions decrease slightly, possibly due to acid or alkaline hydrolysis of the sulfur-containing groups. Chromium is present but in small amounts, which would seem to confirm that there was no adsorption of chromate, because it was retained by electrostatic repulsion instead. Moreover, potassium substituted sodium as the counter-ion for the negative charges.

In short, EDS seems to confirm the presence of PSS on the PVDF membranes and the presence of negative charges on PSS substituting the positive charges on PVDF. Moreover, the shorter penetration into the layer below PSS found for the HFM-183+PSS+Ar-medium membrane could be explained by a consolidation of PVDF plus PSS as a consequence of the plasma treatment.

2.2.5.*Attenuated Total R*eflectance *Fourier Transform Infrared Spectroscopy (FTIR-ATR)*

Figure 10 shows FTIR-ATR results for the HFM-183, HFM-183+PSS and HFM-183+PSS+Ar-medium membranes and compared with FTIR-ATR spectra of a pure PSS film as reported by Li et al. [52].

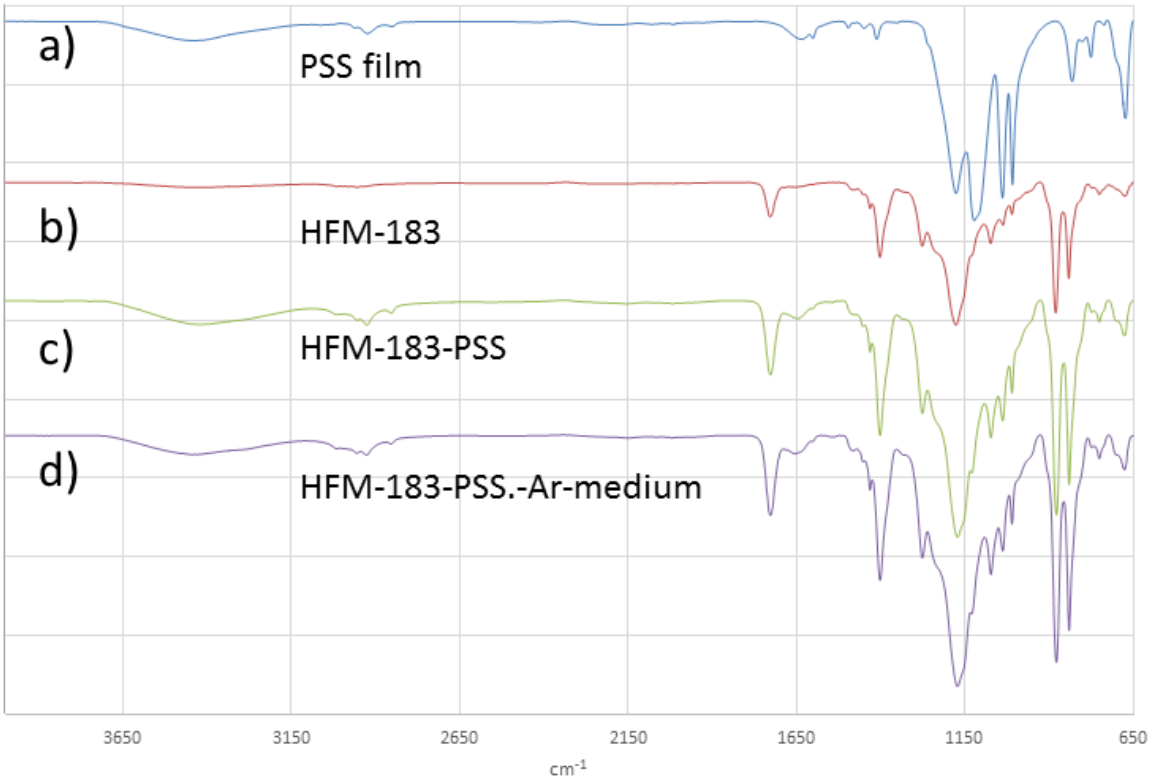

Fig. 10.- FTIR-ATR spectra for: a pure PSS film (a) the HFM-183 membrane (b), the HFM-183+PSS membrane (c) and the HFM-183+PSS+Ar-medium membrane (d).

Referring to the pure PSS film shown in Figure 10a, there are the following peaks in the FTIR-ATR spectrum: from 3700 to 3000 cm^{-1} , a stretching signal due to water vibration; three small peaks around 3100 cm^{-1} corresponding to the stretching of the aromatic (–C=H) groups. At 2920 cm^{-1} there are two signals for stretching vibrations of alkyl groups (C–H); at 1642 cm^{-1} there is a peak linked to the structural water; at 1600, 1500, 1450 and 1410 cm^{-1} there are stretching vibrations of the aromatic ring (–C=C–); at 1180 and 1110 cm^{-1}, stretching asymmetric vibrations of the ($–SO_3^-$) group; at 1040 and 1005 cm^{-1}, symmetric stretching vibrations of the group ($–SO_3^-$), appear. Finally, at 836, 771 and 677 cm^{-1} there are peaks corresponding to out-of-plane (wagging or twisting) vibrations of the (=C–H) group.

In Figure 10b, the spectrum for the HFM-183 membrane is presented. It agrees with those obtained by Bormashenko (for PVDF films) [25] and by Ekambaram (for nanofiltration membranes made of PVDF) [53,54]. Also, there are signals of ammonium ions (NH_4^+) that would confer a positive charge on the membrane, as well as its possible counter-ion, the ion acetate (CH_3COO^-). The chloride ion, however, another possible counter-ion for ammonium, does not show signals in infrared (4000 – 625 cm^{-1}). There is a barely-perceptible signal corresponding to the stretch vibration of the ammonium bonds (N–H). There are a pair of double peaks at 2863 and 2926 cm^{-1} corresponding to the symmetric and asymmetric stretching of the methylene groups ($–CH_2–$) of the polymeric chain. At 1727 cm^{-1} there is a signal of stretching associated with the carbonyl group

(C=O) of the acetate ion. At 1403 cm^{-1} there are scissoring vibrations of methylene groups. From 1435 to 1390 cm^{-1} there is a signal of ammonium ion overlapping, due to the proximity of the signal of methylene groups. From 1260 to 1230 cm^{-1} the stretching vibration associated with the acetate bond (C–O) appears. From 1245 to 1140 cm^{-1} there are out-of-plane signals for the (–C–F) group. At 923 cm^{-1} there is an out-of-plane signal for the (–C–H) group and, finally, at 840 cm^{-1} there is a rocking vibration of methylene groups. Those signals related to membrane charge (ammonium and acetate) have less intensity due to the small amount used, as well as their dispersion in the membrane.

Figures 10c and 10d, present the spectra for HFM-183+PSS and HFM-183+PSS+Ar-medium membranes. In both spectra, the peaks corresponding to –C–F (from HFM-183) and to $-SO_3^-$ (PSS) can be observed. The HFM-183+PSS+Ar-medium membrane does not exhibit either any relevant displacement or changes of the peaks corresponding to PSS ($-SO_3^-$) or to PVDF ($-CH_2-$ and $-CF_2-$). This would seem to rule out any relevant change in PVDF or PSS chains due to the argon-plasma treatment.

Around 1900 cm^{-1} there are weak signals that are hardly observable. Another medium-intensity signal is between 800 and 850 cm^{-1}, which slightly overlaps with the PVDF peak at 840 cm^{-1}. A shoulder can be seen at 830 cm^{-1}. These signals do not appear in the HFM-183+PSS spectrum. This could be attributed to the appearance of new links between PVDF and PSS that could consolidate the composite membrane. This could lead to a certain degree of immobilization or grafting of PSS on PVDF [42–44].

In summary, FTIR-ATR shows that PSS is well-deposited on the HFM-183 (PVDF substrate); moreover, it seems that plasma treatment increases linkage between PSS and PVDF.

3. Conclusions

A new methodology for the modification of PVDF ultrafiltration membranes has been tried and tested for separate anions. The modification in question was performed by filtration of an aqueous PSS solution that led to a deposition of 0.071 g of PSS/cm^2 on the membrane. The membrane obtained was then treated with argon plasma at an intermediate power. Because the original ultrafiltration membrane, HFM-183, was positively charged and PSS is negative, the electrostatic interaction ensured an initial anchoring of the PSS layer. The subsequent plasma treatment consolidated this linkage in such a way that the resulting HFM-183+PSS+Ar-medium membrane showed good stability during long-term water immersion and alkaline and acidic treatments.

The changes on the surfaces after modifications were tested by using zeta potential, FTIR-ATR, SEM, and EDS. They confirmed the formation of supplementary bonds linking PSS on PVDF (HFM-183) and a compaction of PSS after argon-plasma treatment at intermediate powers. This and stability tests showed that after plasma treatment the PSS layer was consolidated. The zeta potential showed a negative charge at pH 3 – 10, remaining practically stable. EDS showed a small presence of chrome on the used membranes, meaning that separation was mainly determined by electrostatic repulsion. Image analyses of the SEM pictures show that the average pore radius decreased after

modification by 60.67% to 5.40 nm. This radius is still big enough to reject any significant effect of size restrictions on the anions.

Due to the negative charge of these modified membranes, they were used to filtrate different anionic solutions of: nitrate, acid chromate, chromate and a mixture of acid/diacid phosphate. These differently-charged anions gave acceptable retentions considering their observed retention coefficients. The corresponding true retention coefficients were quite high, which means that retention should benefit from a more efficient design of module and fluid mechanics. Retention was due to electrostatic effects fundamentally.

We can conclude that after modification, the membranes are rather selective to divalent (or polyvalent) anions. According to zeta potential and membrane performance characterizations, these modified membranes behave like nanofiltration membranes in terms of the retention mechanism and the resulting retention coefficients, but they have the ultrafiltration characteristic of working at lower pressures, with the corresponding savings of energy.

4. Aknowledgements

The authors would like to thank the Spanish "Ministerio de Ciencia e Innovación (MCINN)" for the financial support of this work within the framework of the "Plan Nacional de I + D + I" through the research project MAT2016-76413-C2-R. They are also indebted to the Guanajuato University – CONACYT National Laboratory for SEM – EDS analysis.

Ivette G. Sandoval-Olvera acknowledges the Consejo Nacional de Ciencia y Tecnología (CONACyT - México) for her PhD grant during the August 2012 – July 2017 period (fellowship 273684). She is also grateful to SMAP (Grupo de Superficies y Materiales Porosos) for her research stay at the University of Valladolid in Spain.

5. References

[1] A.M. Yusof, N.A.N.N. Malek, Removal of Cr(VI) and As(V) from aqueous solutions by HDTMA-modified zeolite Y, J. Hazard. Mater. 162 (2009) 1019–1024. doi:10.1016/j.jhazmat.2008.05.134.

[2] W. Song, T. Shi, D. Yang, J. Ye, Y. Zhou, Y. Feng, Pretreatment effects on the sorption of Cr(VI) onto surfactant-modified zeolite: Mechanism analysis, J. Environ. Manage. 162 (2015) 96–101. doi:10.1016/j.jenvman.2015.07.010.

[3] A. Zhitkovich, Chromium in drinking water: Sources, metabolism, and cancer risks, Chem. Res. Toxicol. 24 (2011) 1617–1629. doi:10.1021/tx200251t.

[4] Z. Chen, Y. Li, M. Guo, F. Xu, P. Wang, Y. Du, P. Na, One-pot synthesis of Mn-doped TiO2grown on graphene and the mechanism for removal of Cr(VI) and Cr(III), J. Hazard. Mater. 310 (2016) 188–198. doi:10.1016/j.jhazmat.2016.02.034.

[5] N.M. Dogan, C. Kantar, S. Gulcan, C.J. Dodge, B.C. Yilmaz, M.A. Mazmanci,

Chromium(VI) bioremoval by pseudomonas bacteria: Role of microbial exudates for natural attenuation and biotreatment of Cr(VI) contamination, Environ. Sci. Technol. 45 (2011) 2278–2285. doi:10.1021/es102095t.

[6] X. Zhao, P.A. Sobecky, L. Zhao, P. Crawford, M. Li, Chromium(VI) transport and fate in unsaturated zone and aquifer: 3D Sandbox results, J. Hazard. Mater. 306 (2016) 203–209. doi:10.1016/j.jhazmat.2015.12.004.

[7] Y.M. Tzou, Y.R. Chen, M.K. Wang, Chromate sorption by acidic and alkaline soils, J. Environ. Sci. Heal. Part A. 33 (1998) 1607–1630. doi:10.1080/10934529809376807.

[8] A. Al Mamun, M. Morita, M. Matsuoka, C. Tokoro, Sorption mechanisms of chromate with coprecipitated ferrihydrite in aqueous solution, J. Hazard. Mater. 334 (2017) 142–149. doi:10.1016/j.jhazmat.2017.03.058.

[9] W. Yao, J. Wang, P. Wang, X. Wang, S. Yu, Y. Zou, J. Hou, T. Hayat, A. Alsaedi, X. Wang, Synergistic coagulation of GO and secondary adsorption of heavy metal ions on Ca/Al layered double hydroxides, Environ. Pollut. 229 (2017) 827–836. doi: 10.1016/j.envpol.2017.06.084.

[10] S. Sen, S. Dutta, S. Guhathakurata, J. Chakrabarty, S. Nandi, A. Dutta, Removal of Cr(VI) using a cyanobacterial consortium and assessment of biofuel production, Int. Biodeterior. Biodegrad. 119 (2017) 211–224. doi:10.1016/j.ibiod.2016.10.050.

[11] C. Zhang, Y. Sun, Z. Yu, G. Zhang, J. Feng, Simultaneous removal of Cr(VI) and acid orange 7 from water solution by dielectric barrier discharge plasma, Chemosphere. 191 (2018) 527–536. doi:10.1016/J.CHEMOSPHERE.2017.10.087.

[12] J. Zhang, C. Zhang, G. Wei, Y. Li, X. Liang, W. Chu, H. He, D. Huang, J. Zhu, R. Zhu, Reduction removal of hexavalent chromium by zinc-substituted magnetite coupled with aqueous Fe(II) at neutral pH value, J. Colloid Interface Sci. 500 (2017) 20–29. doi:10.1016/j.jcis.2017.03.103.

[13] K. Xiao, F. Xu, L. Jiang, Z. Dan, N. Duan, The oxidative degradation of polystyrene resins on the removal of Cr(VI) from wastewater by anion exchange, Chemosphere. 156 (2016) 326–333. doi:10.1016/j.chemosphere.2016.04.116.

[14] Y. Gong, L. Gai, J. Tang, J. Fu, Q. Wang, E.Y. Zeng, Reduction of Cr(VI) in simulated groundwater by FeS-coated iron magnetic nanoparticles, Sci. Total Environ. 595 (2017) 743–751. doi:10.1016/j.scitotenv.2017.03.282.

[15] T. Yu, S. Liu, M. Xu, J. Peng, J. Li, M. Zhai, Synthesis of novel aminated cellulose microsphere adsorbent for efficient Cr(VI) removal, Radiat. Phys. Chem. 125 (2016) 94–101. doi: 10.1016/j.radphyschem.2016.03.019.

[16] V. Sinha, N.A. Manikandan, K. Pakshirajan, R. Chaturvedi, Continuous removal of Cr(VI) from wastewater by phytoextraction using Tradescantia pallida plant based vertical subsurface flow constructed wetland system, Int. Biodeterior. Biodegradation. 119 (2017) 96–103. doi: 10.1016/j.ibiod.2016.10.003.

[17] Q.-Y. Chen, R. Fu, X.-W. Fang, W.-F. Cai, Y.-H. Wang, S.-A. Cheng, Cr-methanol fuel cell for efficient Cr(VI) removal and high power production, Appl. Energy. 138 (2015) 31–35. doi: 10.1016/j.apenergy.2014.10.053.

[18] P. Roy Choudhury, S. Majumdar, G.C. Sahoo, S. Saha, P. Mondal, High pressure ultrafiltration CuO/hydroxyethyl cellulose composite ceramic membrane for separation of Cr (VI) and Pb (II) from contaminated water, Chem. Eng. J. 336 (2018) 570–578. doi:10.1016/J.CEJ.2017.12.062.

[19] S. Koushkbaghi, A. Zakialamdari, M. Pishnamazi, H.F. Ramandi, M. Aliabadi, M. Irani, Aminated-Fe3O4 nanoparticles filled chitosan/PVA/PES dual layers nanofibrous membrane for the removal of Cr(VI) and Pb(II) ions from aqueous solutions in adsorption and membrane processes, Chem. Eng. J. (2017). doi:10.1016/J.CEJ.2017.12.075.

[20] Y.-Z. Lu, G.-J. Chen, Y.-N. Bai, L. Fu, L.-P. Qin, R.J. Zeng, Chromium isotope fractionation during Cr(VI) reduction in a methane-based hollow-fiber membrane biofilm reactor, Water Res. 130 (2018) 263–270. doi:10.1016/j.watres.2017.11.045.

[21] M. Kazemi, M. Jahanshahi, M. Peyravi, Hexavalent chromium removal by multilayer membrane assisted by photocatalytic couple nanoparticle from both permeate and retentate, J. Hazard. Mater. 344 (2018) 12–22. doi:10.1016/j.jhazmat.2017.09.059.

[22] M.S. Gaikwad, C. Balomajumder, Simultaneous rejection of fluoride and Cr(VI) from synthetic fluoride-Cr(VI) binary water system by polyamide flat sheet reverse osmosis membrane and prediction of membrane performance by CFSK and CFSD models, J. Mol. Liq. 234 (2017) 194–200. doi:10.1016/j.molliq.2017.03.073.

[23] Z. Yao, S. Du, Y. Zhang, B. Zhu, L. Zhu, A.E. John, Positively charged membrane for removing low concentration Cr(VI) in ultrafiltration process, J. Water Process Eng. 8 (2015) 99–107. doi:10.1016/j.jwpe.2015.08.005.

[24] K.A. Gebru, C. Das, Removal of chromium (VI) ions from aqueous solutions using amine-impregnated TiO2 nanoparticles modified cellulose acetate membranes, Chemosphere. 191 (2018) 673–684. doi:10.1016/j.chemosphere.2017.10.107.

[25] A. Akbari, Z. Derikvandi, S.M. Mojallali Rostami, Influence of chitosan coating on the separation performance, morphology and anti-fouling properties of the polyamide nanofiltration membranes, J. Ind. Eng. Chem. 28 (2015) 268–276. doi:10.1016/j.jiec.2015.03.002.

[26] Y. Wang, H. Lin, Z. Xiong, Z. Wu, Y. Wang, L. Xiang, A. Wu, F. Liu, A silane-based interfacial crosslinking strategy to design PVDF membranes with versatile surface functions, J. Memb. Sci. 520 (2016) 769–778. doi:10.1016/j.memsci.2016.08.029.

[27] R. Reis, L.F. Dum??e, A. Merenda, J.D. Orbell, J.A. Sch??tz, M.C. Duke, Plasma-induced physicochemical effects on a poly(amide) thin-film composite membrane, Desalination. 403 (2017) 3–11. doi:10.1016/j.desal.2016.06.009.

[28] N. Nady, M.C.R. Franssen, H. Zuilhof, M.S.M. Eldin, R. Boom, K. Schroën, Modification methods for poly(arylsulfone) membranes: A mini-review focusing on surface modification, Desalination. 275 (2011) 1–9. doi:10.1016/j.desal.2011.03.010.

[29] H. Zhou, Y. Su, X. Chen, J. Luo, S. Tan, Y. Wan, Plasma modification of substrate with poly(methylhydrosiloxane) for enhancing the interfacial stability of PDMS/PAN composite membrane, J. Memb. Sci. 520 (2016) 779–789. doi:10.1016/j.memsci.2016.08.039.

[30] K.C. Khulbe, C. Feng, T. Matsuura, The art of surface modification of synthetic polymeric

membranes, J. Appl. Polym. Sci. 115 (2010) 855–895. doi:10.1002/app.31108.

[31] A. Tena, L. Palacio, P. Prádanos, A.E. Lozano, A. Marcos-Fernández, A. Hernández, Improving the Permeation Properties by Plasma Surface Modification, Procedia Eng. 44 (2012) 1353–1355. doi:10.1016/j.proeng.2012.08.783.

[32] M.-C. Fournier-Salaün, P. Salaün, Quantitative determination of hexavalent chromium in aqueous solutions by UV-Vis spectrophotometer, Cent. Eur. J. Chem. 5 (2007) 1084–1093. doi:10.2478/s11532-007-0038-4.

[33] E. W. Rice, R. B. Baird, A. D. Eaton Eds., Standard Methods for the Examination of Water and Wastewater, 23rd Ed., American public health association., American water works association and Water environment federation, Washington, USA, (2017). ISBN: 978-0875532875

[34] USEPA, Method 365.3: Phosphorous, All Forms (Colorimetric, Ascorbic Acid, Two Reagent), Cincinnati, OH, 1978. https://www.epa.gov/sites/production/files/2015-08/documents/method_365-3_1978.pdf.

[35] T. Tkavc, I. Petrinič, T. Luxbacher, A. Vesel, T. Ristić, L.F. Zemljič, Influence of O2 and CO2 plasma treatment on the deposition of chitosan onto polyethylene terephthalate (PET) surfaces, Int. J. Adhes. Adhes. 48 (2014) 168–176. doi:10.1016/j.ijadhadh.2013.09.008.

[36] L.M. Robeson, Correlation of separation factor versus permeability for polymeric membranes, J. Memb. Sci. 62 (1991) 165–185. doi:10.1016/0376-7388(91)80060-J.

[37] V.M.M. Lobo, J.L. Quaresma, Handbook of Electrolyte Solutions, Elsevier Science Publishers B.V., Amsterdan, The Netherlands, 1989. ISBN: 0444988475.

[38] G. Velasco, S. Gutiérrez-Granados, C. Ponce De León, A. Alatorre, F.C. Walsh, I. Rodríguez-Torres, The electrochemical reduction of Cr(VI) ions in acid solution at titanium and graphite electrodes, J. Environ. Chem. Eng. 4 (2016) 3610–3617. doi:10.1016/j.jece.2016.08.004.

[39] N. Iadicicco, L. Paduano, V. Vitagliano, Diffusion Coefficients for the System Potassium Chromate−Water at 25 °C, J. Chem. Eng. Data. 41 (1996) 529–533. doi:10.1021/je9502861.

[40] H.D.B. Jenkins, K.P. Thakur, Reappraisal of thermochemical radii for complex ions, J. Chem. Educ. 56 (1979) 576. doi:10.1021/ed056p576.

[41] N. García-Martín, V. Silva, F.J. Carmona, L. Palacio, A. Hernández, P. Prádanos, Pore size analysis from retention of neutral solutes through nanofiltration membranes. The contribution of concentration–polarization, Desalination. 344 (2014) 1–11. doi:10.1016/j.desal.2014.02.038.

[42] Y. Han, S. Song, Y. Lu, D. Zhu, A method to modify PVDF microfiltration membrane via ATRP with low-temperature plasma pretreatment, Appl. Surf. Sci. 379 (2016) 474–479. doi:10.1016/j.apsusc.2016.04.114.

[43] P. Wang, K.L. Tan, E.T. Kang, K.G. Neoh, Plasma-induced immobilization of poly(ethylene glycol) onto poly(vinylidene fluoride) microporous membrane, J. Memb. Sci. 195 (2002) 103–114. doi:10.1016/S0376-7388(01)00548-8.

[44] R.-S. Juang, C. Huang, C.-L. Hsieh, Surface modification of PVDF ultrafiltration membranes by remote argon/methane gas mixture plasma for fouling reduction, J. Taiwan Inst. Chem. Eng. 45 (2014) 2176–2186. doi:10.1016/j.jtice.2014.06.025.

[45] R.I. Peinador, J.I. Calvo, K. ToVinh, V. Thom, P. Prádanos, A. Hernández, Liquid-liquid displacement porosimetry for the characterization of virus retentive membranes, J. Memb. Sci. 372 (2011) 366–372. doi:10.1016/j.memsci.2011.02.022.

[46] N.M. Mokhtar, W.J. Lau, A.F. Ismail, B.C. Ng, Physicochemical study of polyvinylidene fluoride–Cloisite15A® composite membranes for membrane distillation application, RSC Adv. 4 (2014) 63367–63379. doi:10.1039/C4RA10289D.

[47] D. Breite, M. Went, A. Prager, A. Schulze, Tailoring membrane surface charges: A novel study on electrostatic interactions during membrane fouling, Polymers (Basel). 7 (2015) 2017–2030. doi:10.3390/polym7101497.

[48] S.Y. Park, S.H. Choi, J.W. Chung, S.-Y. Kwak, Anti-scaling ultrafiltration/microfiltration (UF/MF) polyvinylidene fluoride (PVDF) membranes with positive surface charges for Ca2+/silica-rich wastewater treatment, J. Memb. Sci. 480 (2015) 122–128. doi:10.1016/j.memsci.2015.01.041.

[49] F. Liu, N.A. Hashim, Y. Liu, M.R.M. Abed, K. Li, Progress in the production and modification of PVDF membranes, J. Memb. Sci. 375 (2011) 1–27. doi:10.1016/j.memsci.2011.03.014.

[50] G. Kang, Y. Cao, Application and modification of poly (vinylidene fluoride)(PVDF) membranes–A review, J. Memb. Sci. 463 (2014) 145–165. doi:10.1016/ j.memsci.2014.03.055.

[51] D. Jan, J.S. Jeon, S. Raghavan, Surface modification of PVDF membranes by grafting of a vinylphosphonium compound, J. Adhes. Sci. Technol. 8 (1994) 1157–1168. doi:10.1163/156856194X01004.

[52] L. Li, R. Ma, N. Iyi, Y. Ebina, K. Takada, T. Sasaki, Hollow nanoshell of layered double hydroxide., Chem. Commun. (Camb). 2 (2006) 3125–3127. doi:10.1039/b605889b.

[53] Y. Bormashenko, R. Pogreb, O. Stanevsky, E. Bormashenko, Vibrational spectrum of PVDF and its interpretation, Polym. Test. 23 (2004) 791–796. doi:10.1016/j.polymertesting. 2004.04.001.

[54] K. Ekambaram, M. Doraisamy, Study on the fabrication, characterization and performance of PVDF/calcium stearate composite nanofiltration membranes, Desalination. 385 (2016) 24–38. doi:10.1016/j.desal.2016.01.029.

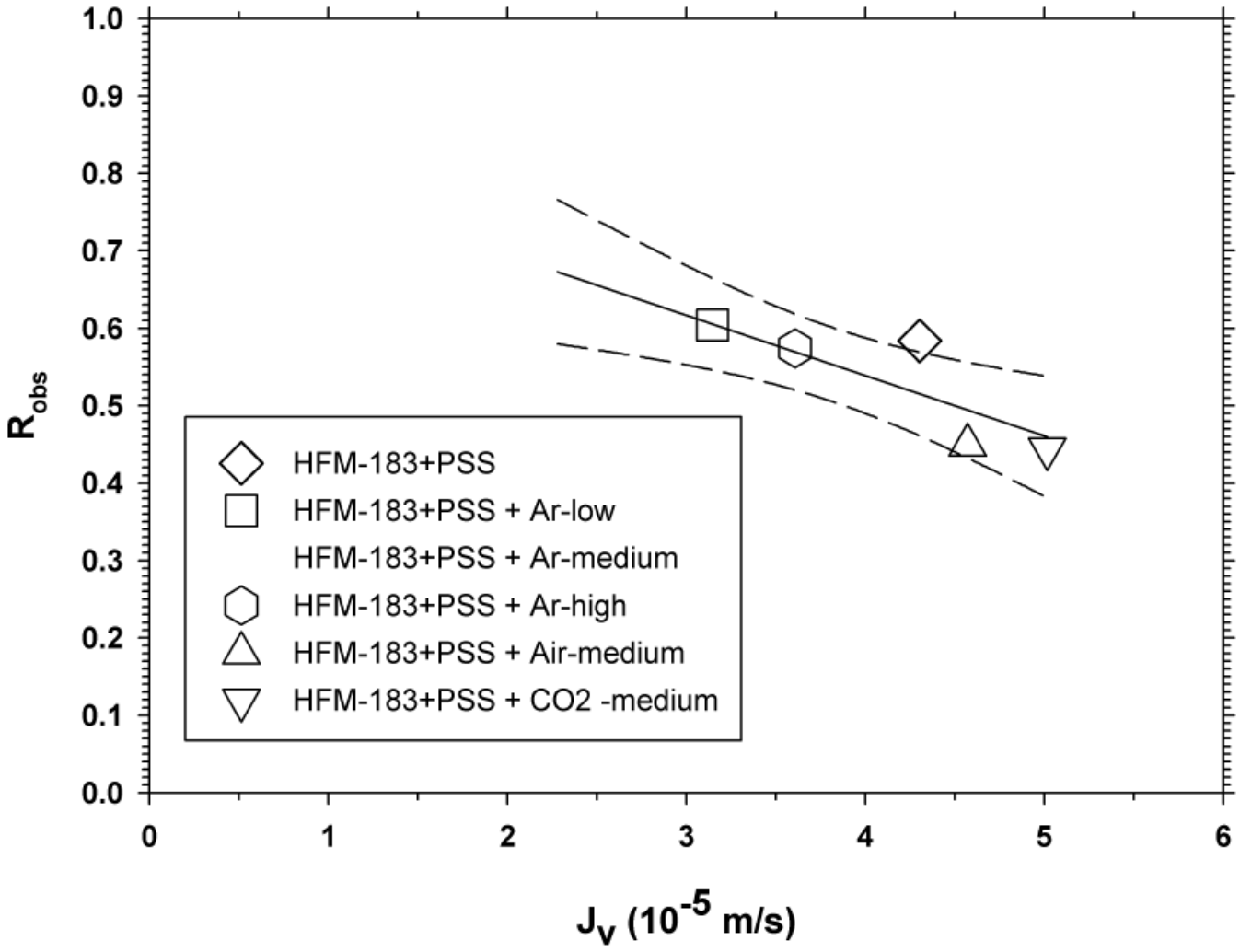

Fig. 1.- Observed retention versus volume flux of chromate solutions for different plasma treatments. Lines correspond to the best straight line fitting the data.

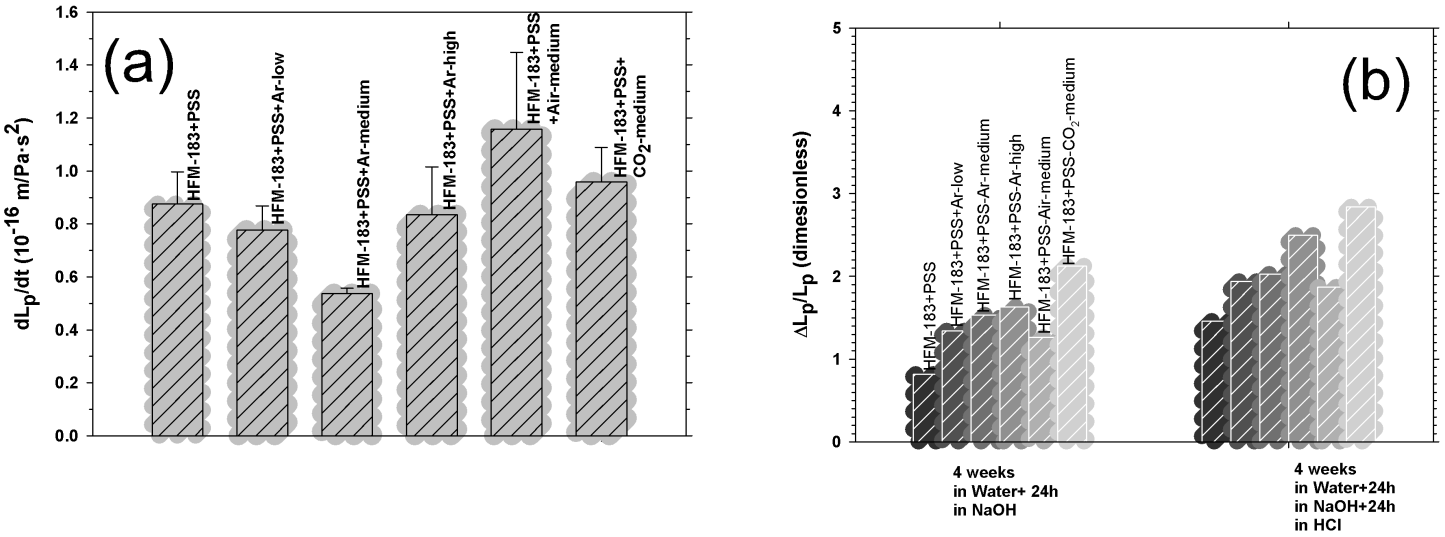

Fig. 2.- a) Water permeability rate of change due to water immersion b) Relative changes in water permeability after alkaline and acidic treatments for different plasma treatments.

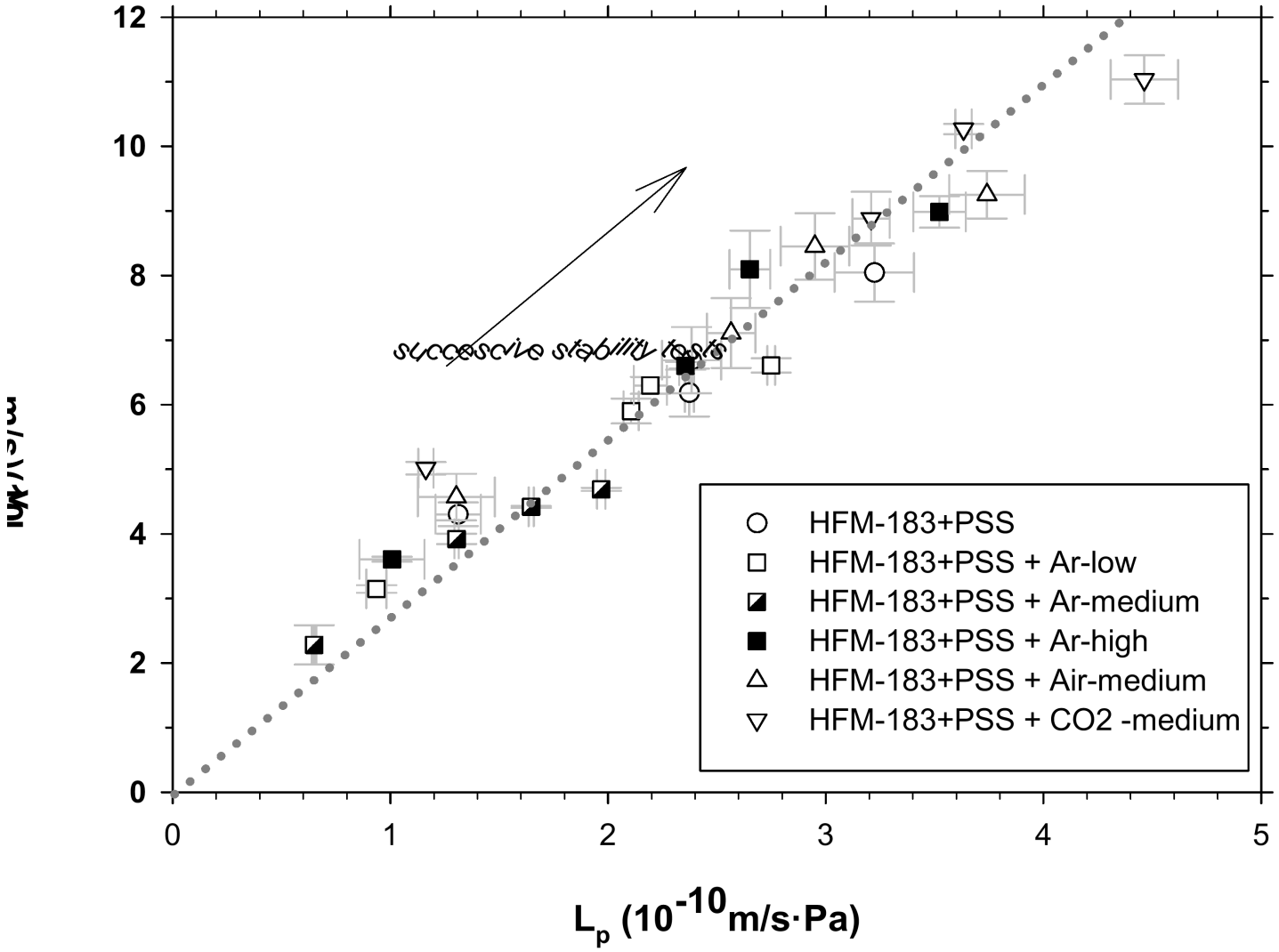

Fig. 3.- Chromate volume fluxes versus water permeabilities.

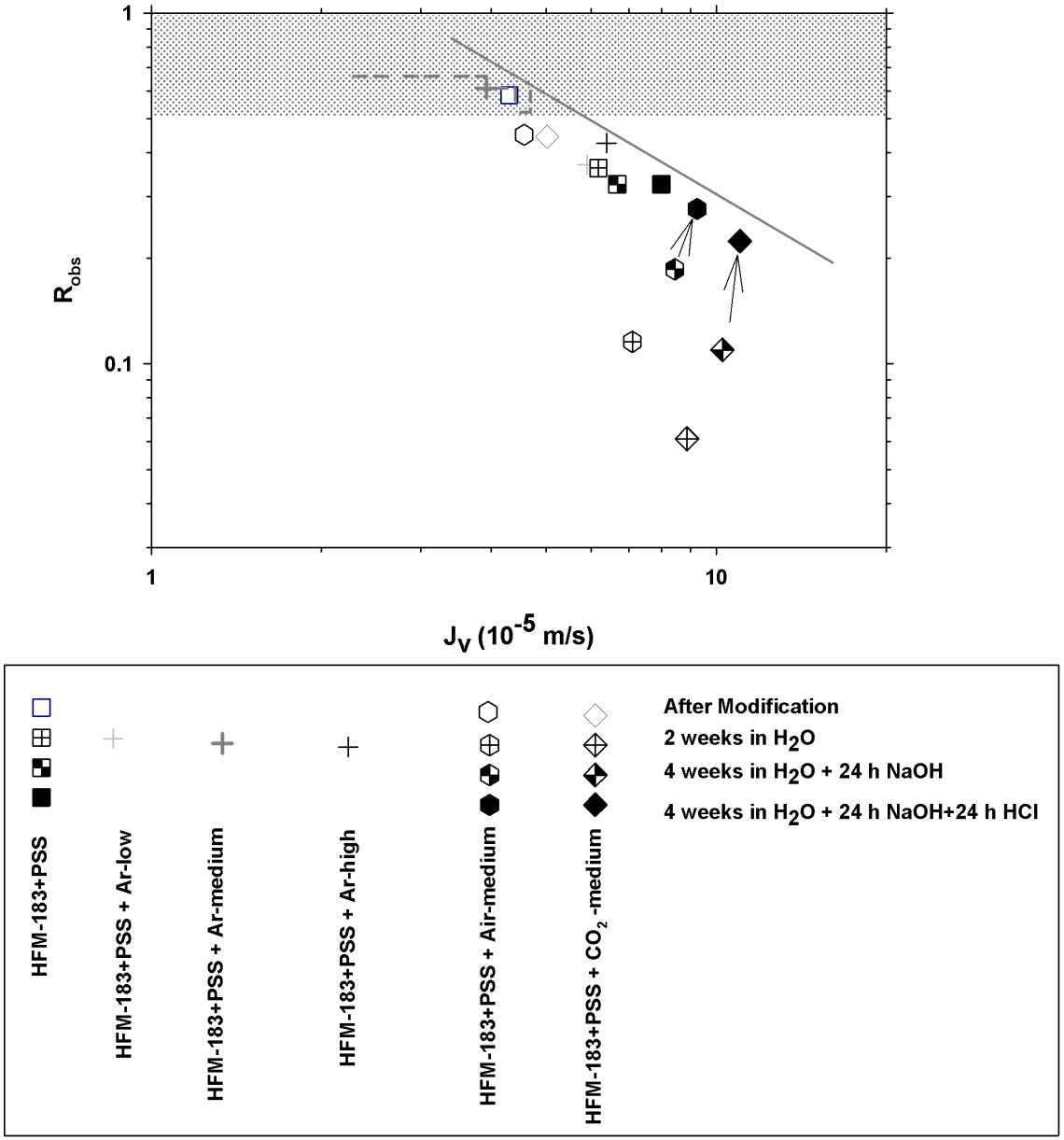

Fig. 4.- Observed retention versus volume flux of chromate solutions for the different plasma treatments before and after their tests for stability.

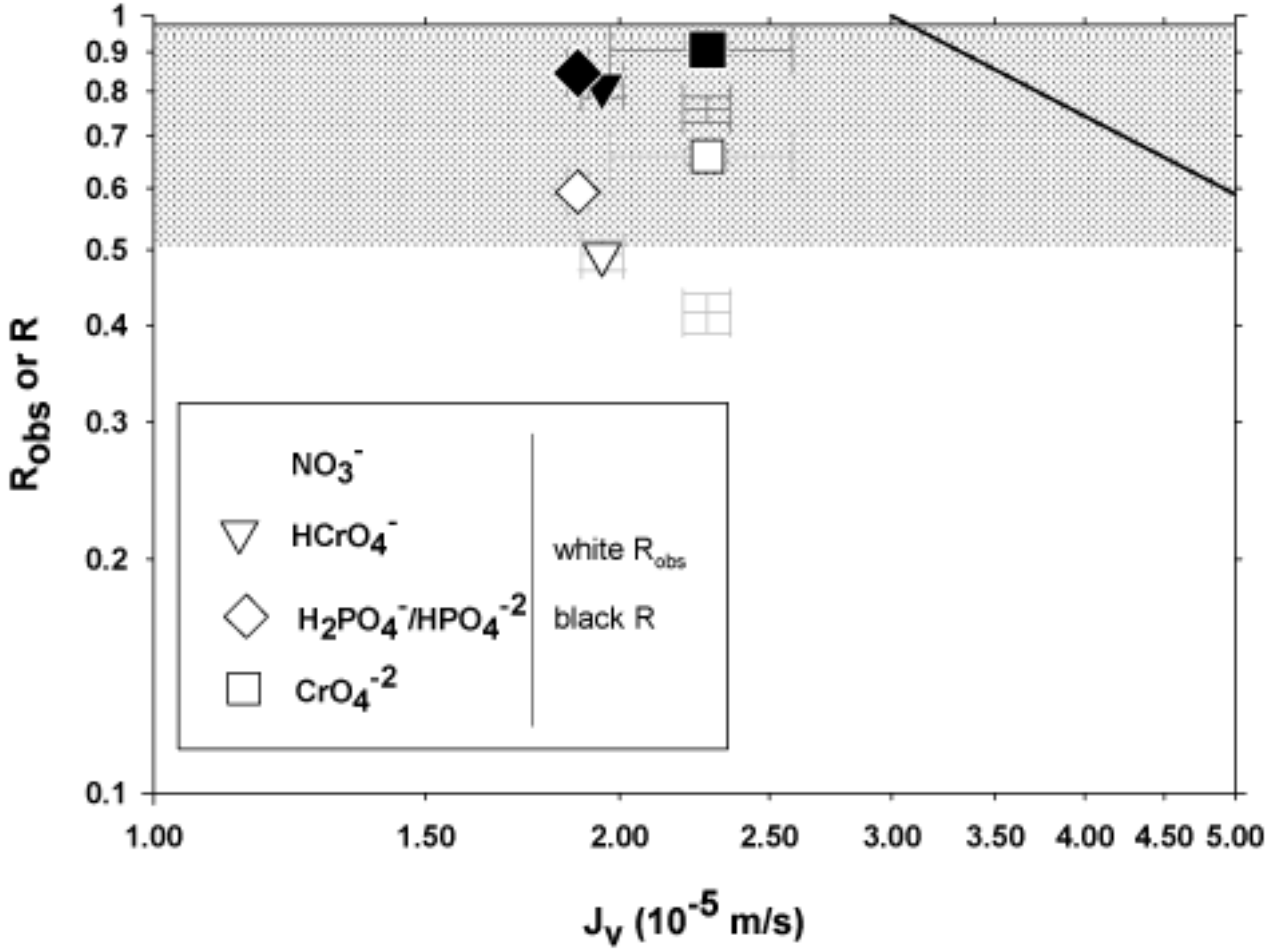

Fig. 5.- Observed and true retention for the HFM-183+PSS+Ar-medium membrane and the anionic solutions used.

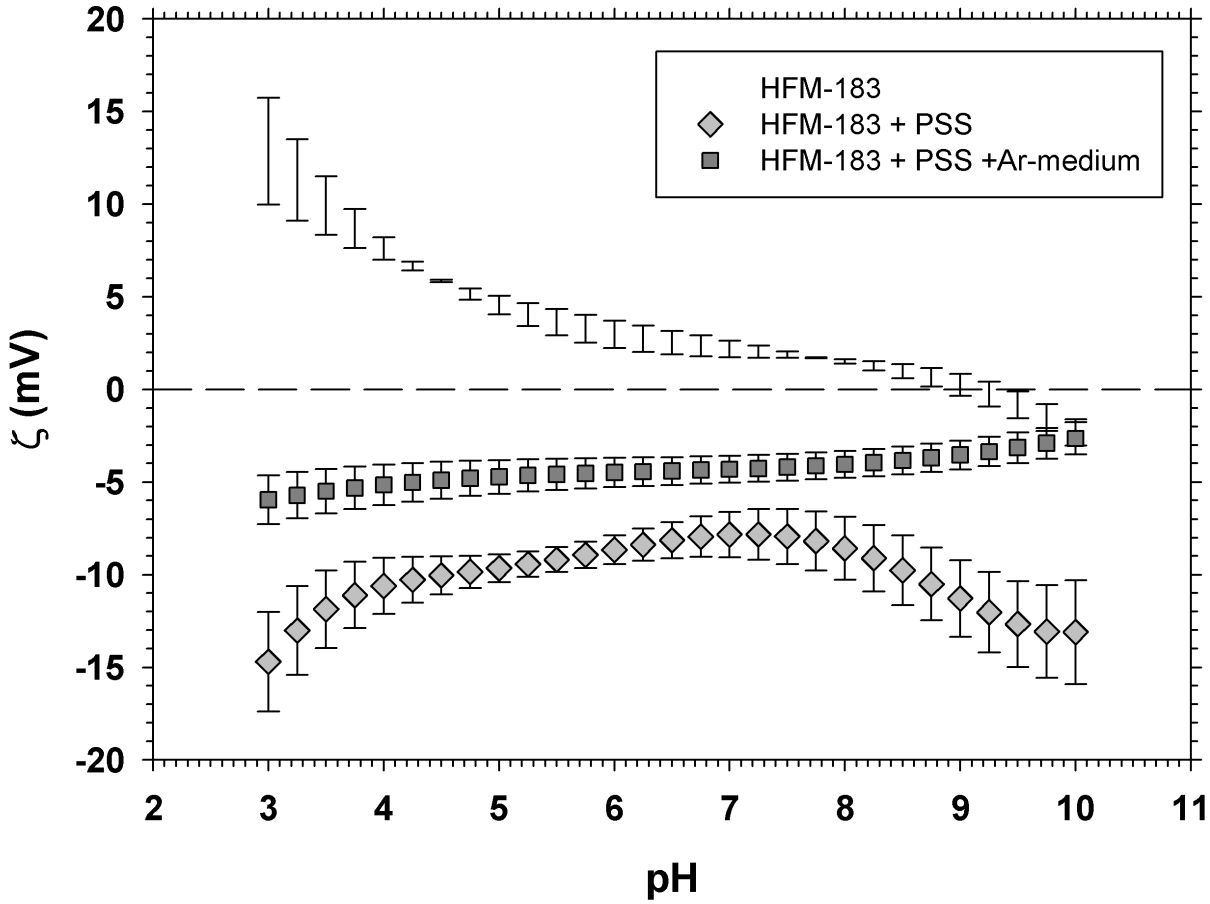

Fig. 6.- Zeta potential vs. pH.

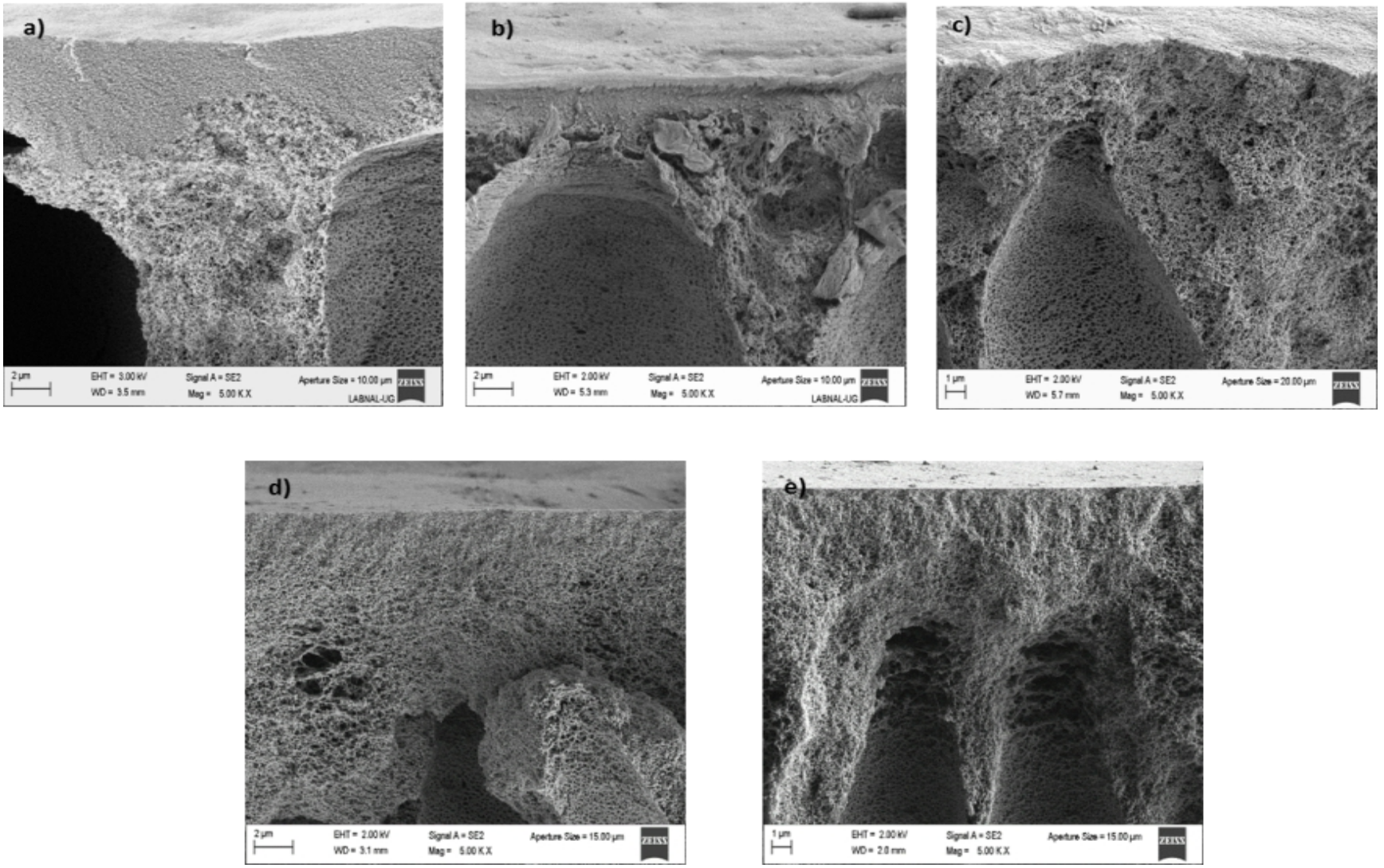

Fig. 7.- SEM pictures of transversal sections of: a) HFM-183, b) HFM-183+PSS, c) HFM-183+PSS+Ar-medium, d) HFM-183+PSS+Ar-medium after chromate filtration and e) HFM-183+PSS+Ar-medium after $HCrO_4^-$ filtration.

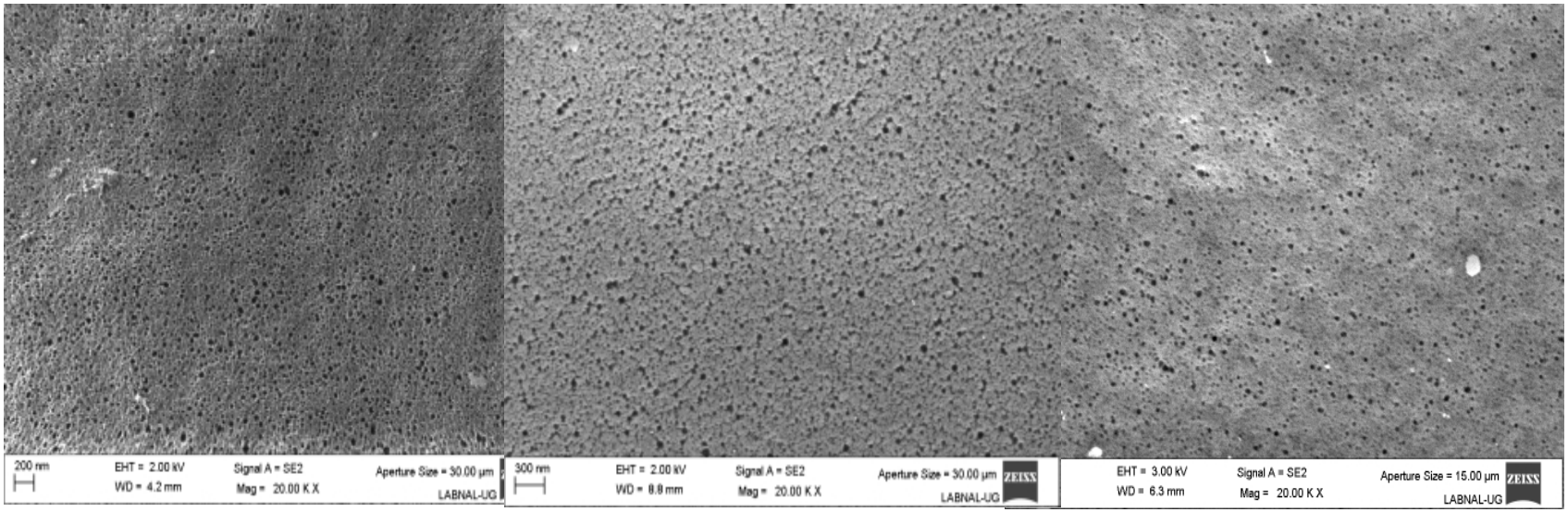

Fig. 8.- Surface SEM image for the membranes: HFM-183 (left), HFM-183+PSS (center) and HFM-183+PSS+Ar-medium (right).

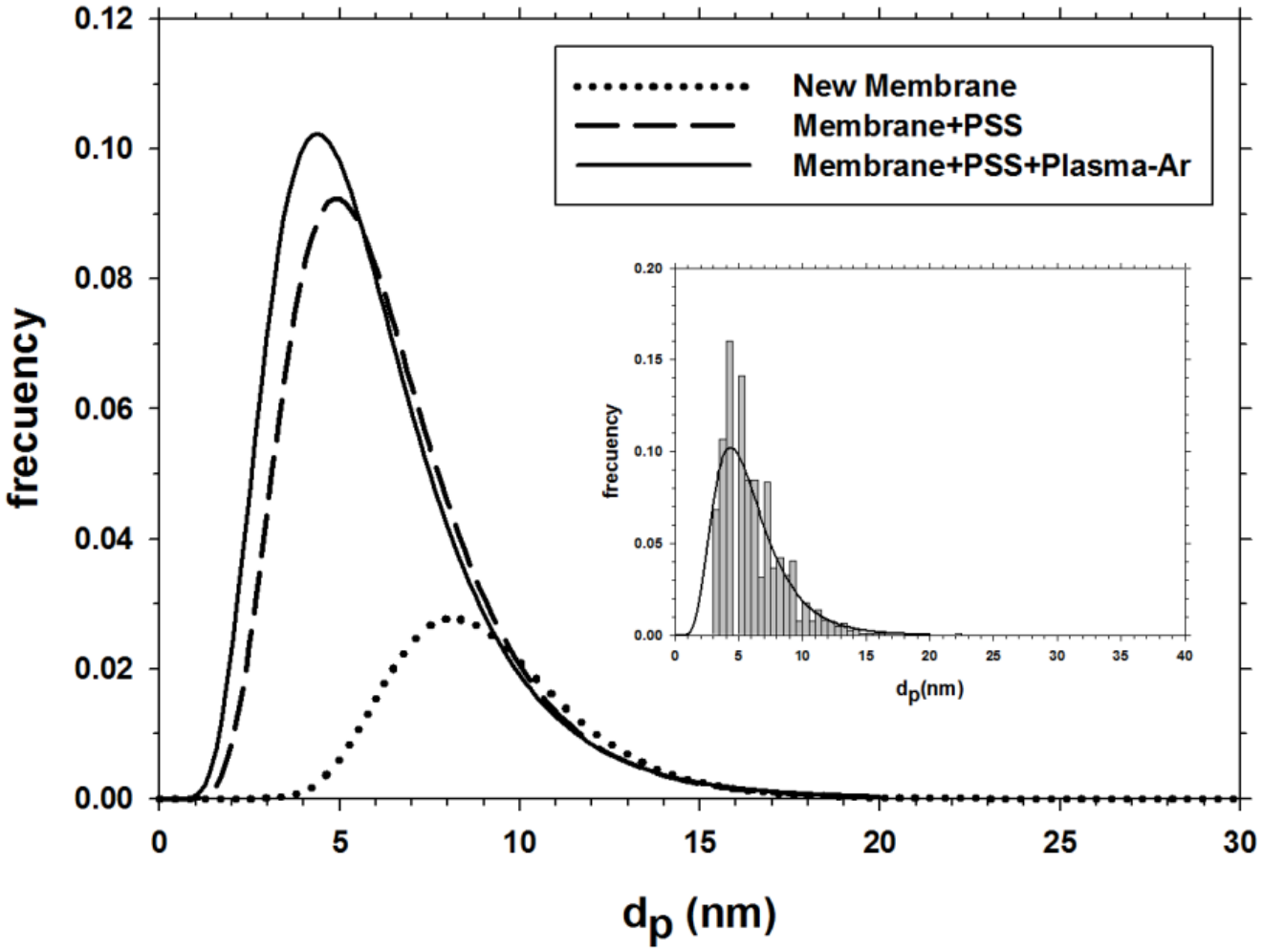

Fig. 9.-Log-normal fitted distribution. The insert shows raw and fitted data for the HFM-183+PSS+Ar-medium membrane.

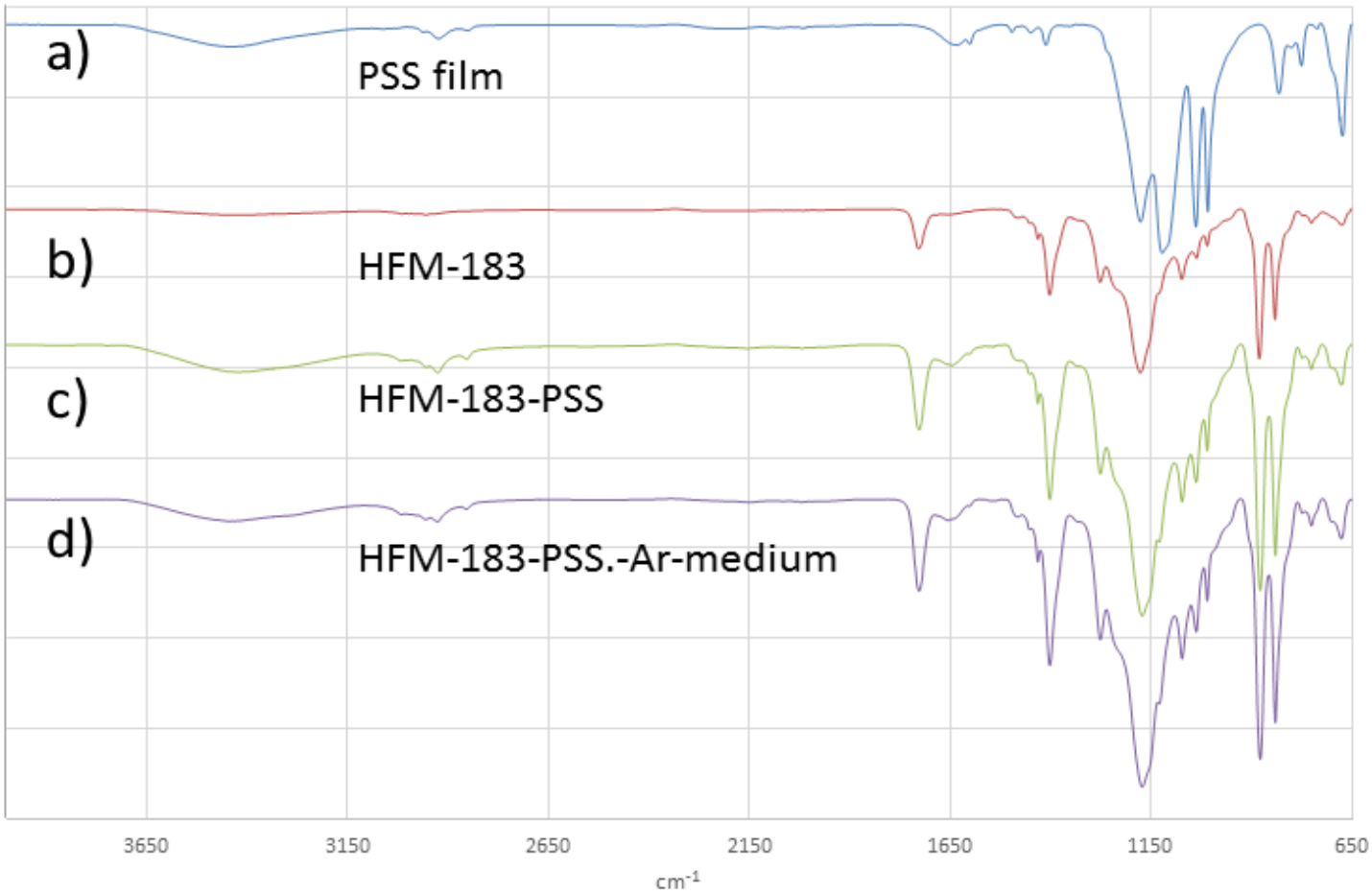

Fig. 10.- FTIR-ATR spectra for: a pure PSS film (a) the HFM-183 membrane (b), the HFM-183+PSS membrane (c) and the HFM-183+PSS+Ar-medium membrane (d).